Article

Immunity

SARS-CoV-2-specific T cell memory with common TCRαβ motifs is established in unvaccinated children who seroconvert after infection

Graphical abstract

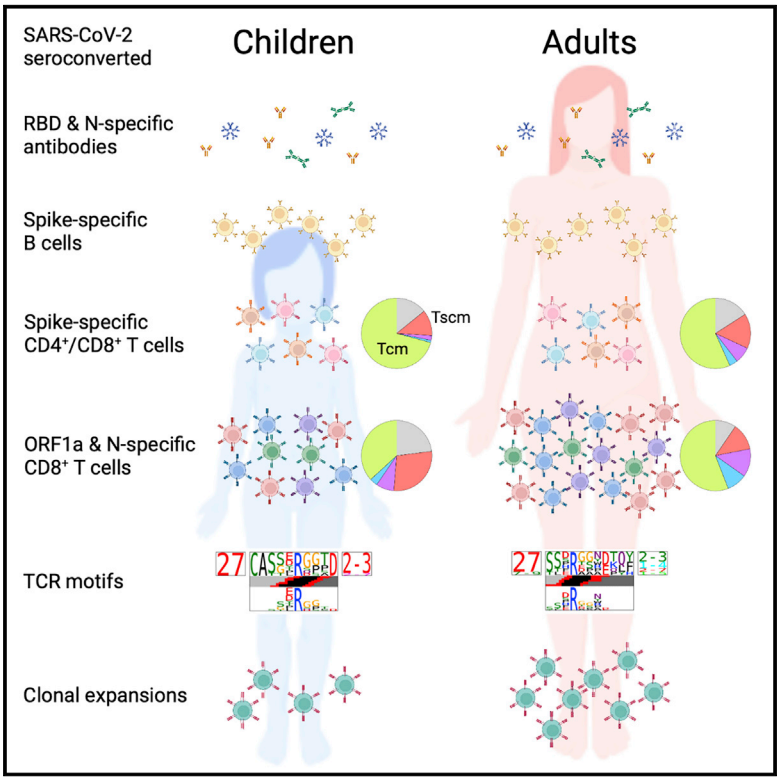

Authors

Louise C. Rowntree, Thi H.O. Nguyen, Lukasz Kedzierski, ..., Nigel W. Crawford, Carolien E. van de Sandt, Katherine Kedzierska

Correspondence

kkedz@unimelb.edu.au

In brief

Children are at lower risk of developing severe COVID-19, yet their primary and memory immune responses are understudied. Rowntree et al. define *ex vivo* $CD8^+$ and $CD4^+$ T cell responses toward SARS-CoV-2 using peptide-HLA tetramers. They find that children have comparable Spike-specific but lower ORF1a- and N-specific memory T cell magnitude with less clonal expansion in comparison with adults.

Highlights

- SARS-CoV-2-specific T cells detected *ex vivo* in unvaccinated seroconverted children
- Comparable Spike-T cell memory responses but lower ORF1a/N-responses found in children
- Reduced clonal expansions within tetramer$^+$ T cells seen in children compared with adults
- Prevalent Tscm phenotype and TCR motif occur in SARS-CoV-2-specific T cells in children

Rowntree et al., 2022, Immunity *55*, 1299–1315
July 12, 2022
https://doi.org/10.1016/j.immuni.2022.06.003

CellPress

Immunity

CellPress
OPEN ACCESS

Article

SARS-CoV-2-specific T cell memory with common TCRαβ motifs is established in unvaccinated children who seroconvert after infection

Louise C. Rowntree,[1,26] Thi H.O. Nguyen,[1,26] Lukasz Kedzierski,[1,2,26] Melanie R. Neeland,[3,4] Jan Petersen,[5] Jeremy Chase Crawford,[6] Lilith F. Allen,[1] E. Bridie Clemens,[1] Brendon Chua,[1] Hayley A. McQuilten,[1] Anastasia A. Minervina,[6] Mikhail V. Pogorelyy,[6] Priyanka Chaurasia,[5] Hyon-Xhi Tan,[1] Adam K. Wheatley,[1,7] Xiaoxiao Jia,[1] Fatima Amanat,[8,9] Florian Krammer,[8,10,11] E. Kaitlynn Allen,[6] Sabrina Sonda,[12] Katie L. Flanagan,[12,13,14,15] Jaycee Jumarang,[16] Pia S. Pannaraj,[16,17] Paul V. Licciardi,[3,4] Stephen J. Kent,[1,7,18] Katherine A. Bond,[1,19] Deborah A. Williamson,[20,21,22] Jamie Rossjohn,[5,23] Paul G. Thomas,[6] Shidan Tosif,[3,4,24] Nigel W. Crawford,[3,4,24,25] Carolien E. van de Sandt,[1,27] and Katherine Kedzierska[1,27,28,*]

[1]Department of Microbiology and Immunology, University of Melbourne, at the Peter Doherty Institute for Infection and Immunity, Melbourne, VIC 3000, Australia
[2]Faculty of Veterinary and Agricultural Sciences, University of Melbourne, Melbourne, VIC 3000, Australia
[3]Infection and Immunity, Murdoch Children's Research Institute, Melbourne, VIC 3000, Australia
[4]Department of Paediatrics, The University of Melbourne, Melbourne, VIC 3000, Australia
[5]Infection and Immunity Program, Department of Biochemistry and Molecular Biology, Biomedicine Discovery Institute, Monash University, Clayton, VIC 3800, Australia
[6]Department of Immunology, St. Jude Children's Research Hospital, Memphis, TN 38105, USA
[7]ARC Centre of Excellence in Convergent Bio-Nano Science and Technology, University of Melbourne, Melbourne, VIC 3000, Australia
[8]Department of Microbiology, Icahn School of Medicine at Mount Sinai, New York, NY 10029, USA
[9]Graduate School of Biomedical Sciences, Icahn School of Medicine at Mount Sinai, New York, NY 10029, USA
[10]Department of Pathology, Molecular and Cell-Based Medicine, Icahn School of Medicine at Mount Sinai, New York, NY 10029, USA
[11]Center for Vaccine Research and Pandemic Preparedness (C-VARPP), Icahn School of Medicine at Mount Sinai, New York, NY 10029, USA
[12]School of Health Sciences and School of Medicine, University of Tasmania, Launceston, TAS 7248, Australia
[13]Department of Immunology and Pathology, Monash University, Commercial Road, Melbourne, VIC 3004, Australia
[14]School of Health and Biomedical Science, RMIT University, Melbourne, VIC 3000, Australia
[15]Tasmanian Vaccine Trial Centre, Clifford Craig Foundation, Launceston General Hospital, Launceston, TAS 7250, Australia
[16]Division of Infectious Diseases, Children's Hospital Los Angeles, Los Angeles, CA 90027, USA
[17]Departments of Pediatrics and Molecular Microbiology and Immunology, Keck School of Medicine of the University of Southern California, Los Angeles, CA 90089, USA
[18]Melbourne Sexual Health Centre, Infectious Diseases Department, Alfred Health, Central Clinical School, Monash University, Melbourne, VIC 3004, Australia
[19]Department of Microbiology, Royal Melbourne Hospital, Melbourne, VIC 3000, Australia
[20]Department of Infectious Diseases, The University of Melbourne at The Peter Doherty Institute for Infection and Immunity, Melbourne, VIC 3000, Australia
[21]Victorian Infectious Diseases Reference Laboratory at The Peter Doherty Institute for Infection and Immunity, Melbourne, VIC 3000, Australia
[22]The Walter and Eliza Hall Institute of Medical Research, Melbourne, VIC 3000, Australia
[23]Institute of Infection and Immunity, Cardiff University School of Medicine, Heath Park, Cardiff CF14 4XN, UK
[24]Department of General Medicine, Royal Children's Hospital Melbourne, Melbourne, VIC 3000, Australia
[25]Royal Children's Hospital Melbourne, Immunisation Service, Melbourne, VIC 3000, Australia
[26]These authors contributed equally
[27]Senior author
[28]Lead contact
*Correspondence: kkedz@unimelb.edu.au
https://doi.org/10.1016/j.immuni.2022.06.003

SUMMARY

As the establishment of severe acute respiratory syndrome coronavirus 2 (SARS-CoV-2)-specific T cell memory in children remains largely unexplored, we recruited convalescent COVID-19 children and adults to define their circulating memory SARS-CoV-2-specific $CD4^+$ and $CD8^+$ T cells prior to vaccination. We analyzed epitope-specific T cells directly *ex vivo* using seven HLA class I and class II tetramers presenting SARS-CoV-2 epitopes, together with Spike-specific B cells. Unvaccinated children who seroconverted had comparable Spike-specific but lower ORF1a- and N-specific memory T cell responses compared with adults. This agreed with our TCR sequencing data showing reduced clonal expansion in children. A strong stem cell memory phenotype and

common T cell receptor motifs were detected within tetramer-specific T cells in seroconverted children. Conversely, children who did not seroconvert had tetramer-specific T cells of predominantly naive phenotypes and diverse TCR$\alpha\beta$ repertoires. Our study demonstrates the generation of SARS-CoV-2-specific T cell memory with common TCR$\alpha\beta$ motifs in unvaccinated seroconverted children after their first virus encounter.

INTRODUCTION

A paradox of the severe acute respiratory syndrome coronavirus 2 (SARS-CoV-2) pandemic is that the majority of children develop less severe coronavirus disease 2019 (COVID-19) (CDC COVID-Response Team, 2020; Chou et al., 2022; O'Driscoll et al., 2021) and have lower secondary attack rates compared with adults and the elderly (Zhu et al., 2021). This is in stark contrast with other respiratory viruses, which often cause severe disease in children (Jansen et al., 2007; Short et al., 2018). The rapid spread of the SARS-CoV-2 Omicron variant, in combination with vaccination of adults and the elderly, has increased the risk of infections in unvaccinated children (Delahoy et al., 2021; Mallapaty, 2021). Despite approvals of COVID-19 vaccines for children, global vaccination rates in children remain low. As immunity to SARS-CoV-2 in children is greatly understudied, it is important to define immunological memory responses generated in SARS-CoV-2 infected, unvaccinated children following their first antigenic encounter.

Children's innate immunity contributes to the rapid resolution of SARS-CoV-2 infection (Neeland et al., 2021a, 2021b). However, children can develop relatively low Spike (S)1-specific immunoglobulin G (IgG) and IgA antibody titers, mainly detected in saliva (Tosif et al., 2020), and reduced seroconversion compared with adults with mild COVID-19 (37% versus 76.2%), despite similar viral loads (Toh et al., 2022). However, a recent large cohort study demonstrated similar neutralization and S-specific antibodies in children and adults (Dowell et al., 2022). Our previous study indicated that children were more likely to mount *de novo* humoral responses following SARS-CoV-2 infection, in contrast to adults and the elderly. Pre-pandemic children had encountered fewer seasonal coronavirus exposures compared with elderly individuals, resulting in less-experienced, polyreactive, and functionally distinct humoral immunity (Selva et al., 2021).

A limited number of studies showed significantly reduced $CD4^+$ and $CD8^+$ T cell responses following stimulation with overlapping SARS-CoV-2 peptide pools in children with mild COVID-19 compared with adults (Cohen et al., 2021; Goenka et al., 2021; Moratto et al., 2020; Pierce et al., 2020). Interferon-γ (IFN-γ) ELISpot analysis with a mix of overlapping peptides to S, nucleocapsid (N), and membrane (M) revealed relatively lower cellular responses to N- and M-derived peptides in children but 2-fold increased responses against S-derived peptides (Dowell et al., 2022). Similarly, stimulation with overlapping peptides in an IFN-γ intracellular cytokine secretion assay showed lower $CD8^+$ and $CD4^+$ T cell responses to SARS-CoV-2 structural and ORF1ab proteins in SARS-CoV-2-infected children compared with adults, despite comparable T cell polyfunctionality (Cohen et al., 2021). Asymptomatic and symptomatic children display similar frequencies of antigen-specific $CD8^+$ T cells, detected by fluorescent intercellular adhesion molecule (ICAM)-1 multimers (Cotugno et al., 2021). Studies in children with multisystem inflammatory syndrome (MIS-C) and SARS-CoV-2 convalescent controls found similar $CD4^+$ and $CD8^+$ T cell responses using peptide megapools and activation-induced marker (AIM) assay (Hsieh et al., 2022). However, importantly, differential T cell responses between children and adults detected by peptide stimulation and functional readouts can also reflect differences in antigen presentation and/or functionality of T cells. Concrete immunological data on the magnitude, phenotype, underlying T cell receptor (TCR) features of SARS-CoV-2 epitope-(peptide + human leukocyte antigen [HLA])-specific $CD8^+$ and $CD4^+$ T cells following the natural SARS-CoV-2 infection of children with asymptomatic or mild COVID-19 are still missing.

Peptide (p)-HLA multimers can accurately track SARS-CoV-2-specific $CD8^+$ and $CD4^+$ T cells directly *ex vivo* during acute and memory time points (Koutsakos et al., 2019; Nguyen et al., 2021a, 2021b), without any *in vitro* manipulations, providing core evidence on key features of virus-specific T cell immunity. Using p-HLA tetramers, we previously demonstrated that pre-pandemic children display a largely naive SARS-CoV-2-specific $CD8^+$ T cell phenotype directed at immunodominant HLA-B7/N_{105} and subdominant HLA-A2/S_{269} epitopes, suggesting a lack of pre-existing memory $CD8^+$ T cell responses (Habel et al., 2020; Nguyen et al., 2021b). However, when it comes to the mild or asymptomatic clinical presentation of COVID-19 in children, the immunological data on SARS-CoV-2 epitope-specific $CD8^+$ and $CD4^+$ T cell immunity are largely non-existent.

Our present study investigated circulating SARS-CoV-2-specific $CD4^+$ and $CD8^+$ T cells within peripheral blood mononuclear cells (PBMCs), as well as B cell immune responses, in 53 children at around one month after mild or asymptomatic SARS-CoV-2 infection or exposure, in comparison with convalescent adults' immune responses. We analyzed SARS-CoV-2-specific T and B cell responses directly *ex vivo*, using seven SARS-CoV-2 tetramers, including six prominent HLA class I (HLA-A*01:01, -A*02:01, -A*03:01, -A*24:02, -B*07:02, and -B*40:01) and one class II (HLA-DPB*04:01) alleles and S-specific B cell probes. Those SARS-CoV-2 epitopes were highly conserved across the major SARS-CoV-2 variants of concern (VOCs). We profiled epitope-specific $CD8^+$ and $CD4^+$ T cell responses at quantitative, phenotypic, and clonal levels to understand their memory potential and found that seroconverted children had memory T cell and B cell profiles, although lower in magnitude compared with seroconverted adults. Additionally, children's SARS-CoV-2-specific T cells displayed similar TCR gene usage but fewer clonal expansions and common motifs compared with adults. Our study provides evidence that seroconverted children generate circulating memory $CD4^+$ and $CD8^+$ T cells, albeit at a lower magnitude compared with seroconverted adults. A small population of mostly SARS-CoV-2-exposed seronegative children had naive tetramer-specific T cells and diverse TCR$\alpha\beta$ usage.

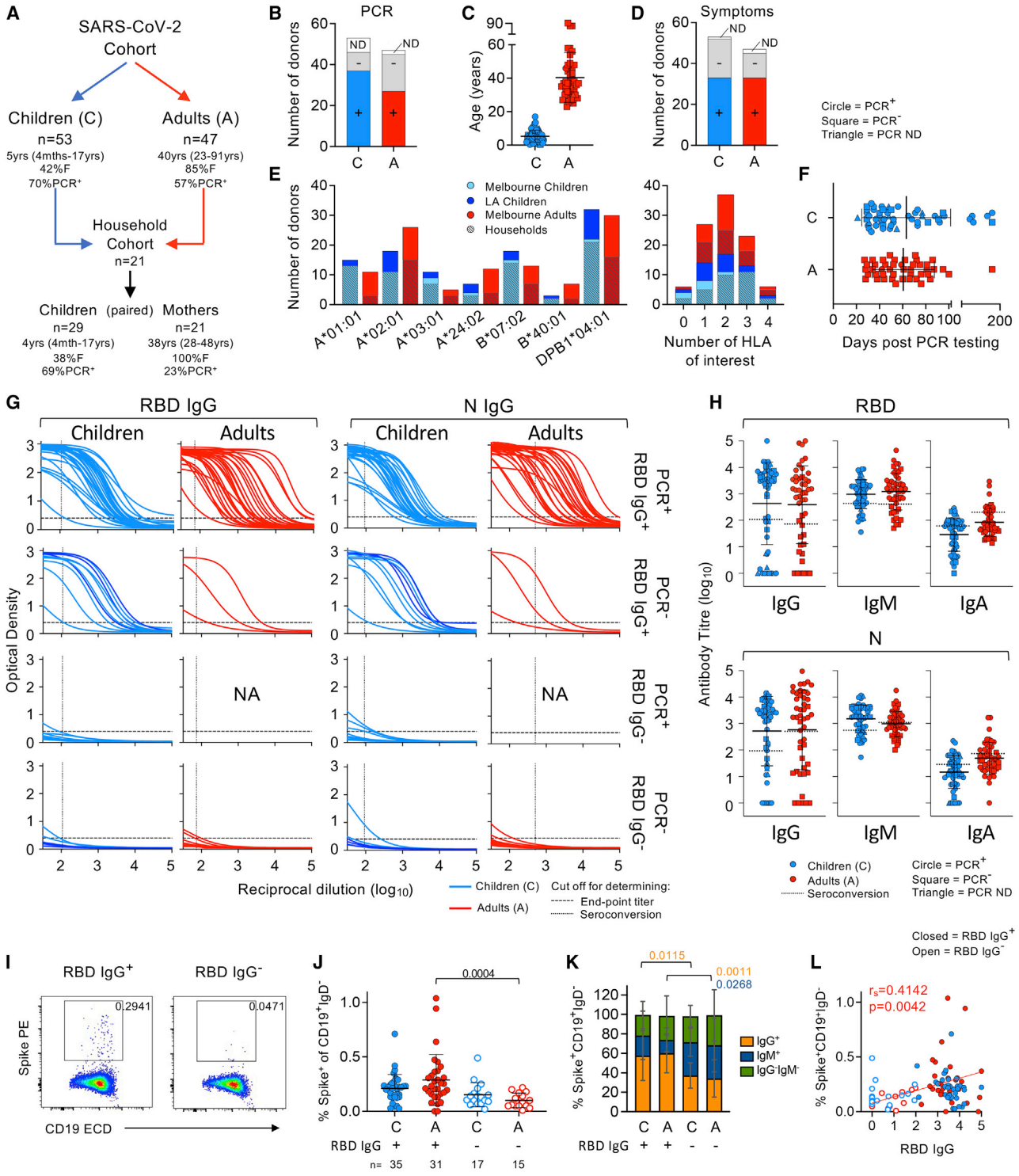

Figure 1. SARS-CoV-2-specific antibody responses and B cell signatures detected in SARS-CoV-2 exposed children and adults

(A) Cohort of SARS-CoV-2 exposed children and adults.

(B) Number of participants who tested SARS-CoV-2 PCR positive, negative, or were undetermined or untested (ND).

(C) Age of SARS-CoV-2 exposed children (n = 53) and adults (n = 47). Data are shown as mean with SD.

(D) Number of children and adults with 2 or more symptoms between days −2 and +14 of PCR testing, no symptoms or were undetermined/untested (ND).

(E) Number of individuals with each HLA of interest (left) and number of simultaneous HLAs of interest (right).

(F) Distribution of days post PCR testing in children and adults (mean, SD).

(G) SARS-CoV-2 RBD- and N-specific IgG dilution curves with participants designated according to PCR and RBD IgG ELISA status (NA, not available).

(legend continued on next page)

RESULTS

COVID-19 children and adult cohort and seroconversion

We recruited 53 children from Melbourne (Australia) and Los Angeles (USA), including 11 sets of siblings and 47 adults (Figure 1A; Table S1). 37 children and 30 adults were PCR positive for SARS-CoV-2 (Figure 1B). 21 mothers were recruited from the same households of which 5 were SARS-CoV-2 PCR positive. All donors were recruited prior to COVID-19 vaccination. Children's mean age was 5 years (range 4 months to 17 years; 42% female), whereas adults' mean age was 40 years (range 23–91 years; 85% female) (Figure 1C; Table S1). 33 children and 33 adults exhibited 2+ symptoms days −2–14 from PCR testing (Figure 1D). None were hospitalized during their infectious period. HLA typing revealed 7 prominent HLA alleles where class I/II tetramers were available (Habel et al., 2020; Minervina et al., 2022; Mudd et al., 2022; Nguyen et al., 2021b; Peng et al., 2020; Rowntree et al., 2021b; Saini et al., 2021; Schulien et al., 2021). High prevalence of class I HLA-A*01:01 (26%), HLA-A*02:01 (44%), HLA-A*24:02 (19%), HLA-B*07:02 (31%), and class II DPB1*04:01 (62%) was found, with 93/100 participants having ≥1 HLA of interest (Figure 1E). Blood was collected at ∼62 days post PCR testing (range 21–180 days) (Figure 1F).

We first measured receptor-binding domain (RBD)- and N-specific IgG, IgM, and IgA antibody titers in COVID-19 convalescent children and adults, and 20 age-matched healthy donors (Figure 1G). 36 children and 32 adults were positive for RBD IgG, while 40 and 29, respectively, were positive for N IgG (Figure 1H). Antibodies positively correlated with each other in both children and adults (children: $r_s = 0.8042$, $p < 0.0001$; adults: $r_s = 0.9033$, $p < 0.0001$) (Figure S1A). RBD IgG antibody titers did not correlate with age or days post PCR testing in children but weakly correlated with days post testing in adults ($r_s = 0.3872$, $p = 0.0072$) (Figure S1BC). 26 children and 29 adults were PCR$^+$ and RBD IgG$^+$. 10 children and 3 adults were PCR-negative, inconclusive, or untested but were all RBD IgG$^+$ (Figure 1G). 11 children were PCR$^+$ but RBD IgG$^-$. 6 were PCR$^-$ and RBD IgG$^-$. The remaining 14 adults were PCR$^-$ and RBD IgG$^-$. RBD-specific IgG titers significantly correlated with IgM and IgA titers in children and adults (IgM children: $r_s = 0.6995$, $p < 0.0001$; adults: $r_s = 0.7777$, $p < 0.0001$; IgA children: $r_s = 0.7490$, $p < 0.0001$; and adults: $r_s = 0.7884$, $p < 0.0001$) (Figure S1D). As anti-SARS-CoV-2-S2 IgG can be more sensitive than anti-RBD IgG in identifying asymptomatic COVID-19 patients (Liao et al., 2021), we measured anti-S2 titers in our cohort. RBD IgG and S2 IgG endpoint titers significantly correlated in children and adults (children: $r_s = 0.7997$, $p < 0.0001$; adults: $r_s = 0.8834$, $p < 0.0001$); however, none of the IgG RBD$^-$ children or adults were S2-seropositive (Figure S1E). Finally, IgG antibodies in children and mothers bound the Delta variant RBD (Figure S1F), indicating cross-protective immunity between ancestral and Delta SARS-CoV-2 strains.

Spike-specific B cells in seroconverted children and adults are predominantly IgG

Using Spike fluorescent probes (Juno et al., 2020; Nguyen et al., 2021b) (Figures 1I and S1G), we found no difference in the frequency of circulating Spike-specific B cells between RBD IgG$^+$ children and adults (Figure 1J). Spike-specific B cells were significantly higher in RBD IgG$^+$ adults compared with RBD IgG$^-$ adults ($p = 0.0004$), but they were not significantly higher between children. Spike$^+$ B cells from RBD IgG$^+$ individuals were mainly of IgG isotype compared with RBD IgG$^-$ individuals (children $p = 0.0115$; adults $p = 0.0011$), with IgM significantly enriched in RBD IgG$^-$ adults ($p = 0.0268$) (Figure 1K). There were no differences in the phenotype of Spike$^+$ B cells between RBD IgG$^+$ and RBD IgG$^-$ individuals (Figure S1H). Spike-specific B cells positively correlated with RBD IgG titers in adults ($r_s = 0.4142$, $p = 0.0042$) (Figure 1L).

Overall, 68% of children and 68% of adults seroconverted at convalescence, and these individuals established SARS-CoV-2-specific B cell memory.

SARS-CoV-2 epitope-specific CD8$^+$ and CD4$^+$ T cell responses are lower in seroconverted children compared with adults

To understand circulating SARS-CoV-2-specific T cell responses in children versus adults, we used tetramer-associated magnetic enrichment (TAME) to measure CD8$^+$ T cells against 6 epitopes *ex vivo* (A1/ORF1a$_{1637}$, A2/S$_{269}$, A3/N$_{361}$, A24/S$_{1208}$, B7/N$_{105}$, and B40/N$_{322}$) (Ferretti et al., 2020; Habel et al., 2020; Nguyen et al., 2021b; Rowntree et al., 2021b; Saini et al., 2021; Schulien et al., 2021) and CD4$^+$ T cells against 1 DPB4/S$_{167}$ epitope (Mudd et al., 2022; Figures 2A and S2A). TAMEs were performed on 46 children and 61 adults (Nguyen et al., 2021b). These SARS-CoV-2 epitopes are restricted by predominant HLA alleles in our cohort and are highly conserved across SARS-CoV-2 VOC (Figure S2B).

Circulating SARS-CoV-2-tetramer$^+$ CD8$^+$ and CD4$^+$ T cells had lower mean frequencies in RBD IgG$^+$ children compared with adults. When pooling all 7 epitopes, RBD IgG$^+$ children had ∼3.35-fold lower mean SARS-CoV-2-specific T cell frequency (3.38×10^{-5}) compared with adults (1.13×10^{-4}, $p = 0.0478$) (Figure 2B). The mean SARS-CoV-2-specific T cell frequency in RBD IgG$^+$ adults was significantly higher than in RBD IgG$^-$ adults (1.08×10^{-5}, $p < 0.0001$) and trended

(H) RBD- and N-specific IgG, IgM, and IgA antibody endpoint titers in children and adults (mean, SD).
(I) Staining profile of class-switched B cells (CD19$^+$IgD$^-$) with Spike probe in seroconverted (RBD IgG$^+$ from ELISA) and non-seroconverted (RBD IgG$^-$) individuals.
(J) Frequencies of Spike$^+$ B cells as a proportion of CD19$^+$IgD$^-$ B cells in PBMCs from RBD IgG$^+$ or IgG$^-$ children and adults; data are shown as median with IQR. The statistical significance was determined with Kruskal-Wallis test.
(K) Isotype distribution of Spike$^+$ B cells from RBD IgG$^+$ or IgG$^-$ children and adults (mean, SD). The statistical significance was determined with Sidak's multiple comparisons test.
(L) Correlation of Spike$^+$ B cells against RBD IgG endpoint titers in SARS-CoV-2 exposed children and adults. The statistical significance was determined using Spearman's rank correlation (r_s).
See also Figure S1.

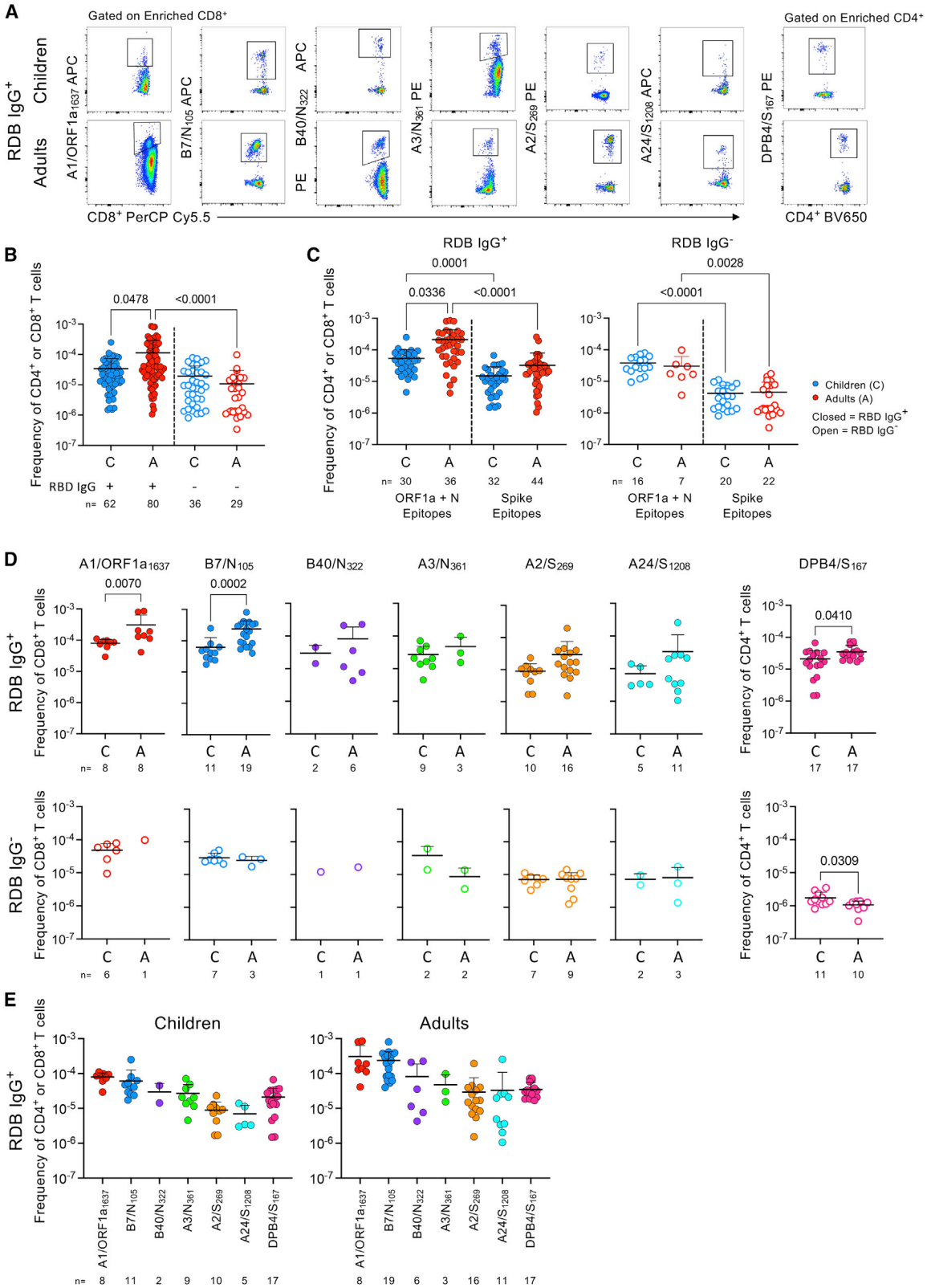

Figure 2. Increased SARS-CoV-2 epitope-specific CD4⁺ and CD8⁺ T cells in SARS-CoV-2 exposed children and adults

Ex vivo analysis of A1/ORF1a$_{1637}$-, B7/N$_{105}$-, B40/N$_{322}$-, A3/N$_{361}$-, A2/S$_{269}$-, and A24/S$_{1208}$-specific CD8⁺ and DPB4/S$_{167}$-specific CD4⁺ T cells from SARS-CoV-2 exposed children and adults. Between one and four epitopes were examined per individual.

(legend continued on next page)

the same way in children (RBD IgG$^+$: 3.38 × 10^{-5}, RBD IgG$^-$: 1.92 × 10^{-5}). Lower frequencies in children suggest that SARS-CoV-2 T cell responses may not have been fully activated/expanded to a similar extent as adults. SARS-CoV-2-specific T cell frequencies weakly correlated with age (r_s = 0.1966, p = 0.0190) in RBD IgG$^+$ individuals (Figure S2C) but not with days post infection (Figure S2D).

As reduced CD4$^+$ and CD8$^+$ T cell responses have been found toward overlapping SARS-CoV-2 peptide pools derived from internal proteins but not Spike-derived peptides in children (Cohen et al., 2021; Goenka et al., 2021; Moratto et al., 2020; Pierce et al., 2020; Dowell et al., 2022), we analyzed T cell responses according to Spike (A2/S_{269}, A24/S_{1208}, and DPB4/S_{167}) or internal (A1/ORF1a$_{1637}$, A3/N_{361}, B7/N_{105}, and B40/N_{322}) epitopes. RBD IgG$^+$ children had ~3.94-fold lower ORF1a- and N-specific T cell mean frequency (5.39 × 10^{-5}) than RBD IgG$^+$ adults (2.121 × 10^{-4}, p = 0.0336) (Figure 2C). Mean frequencies of Spike-specific T cells were lower than internal epitopes in children and adults for both serogroups.

Individually, A1/ORF1a$_{1637}$ and B7/N_{105} CD8$^+$ T cell frequencies were significantly lower in RBD IgG$^+$ children than in adults (Figure 2D). Conversely, RBD IgG$^-$ children and adults had comparable CD8$^+$ T cell frequencies for all epitopes. DPB4/S_{167}-specific CD4$^+$ T cells were higher in RBD IgG$^+$ adults than in children (p = 0.0410), but this was reversed in RBD IgG$^-$ individuals (p = 0.0309). A1/ORF1a$_{1637}$ and B7/N_{105} CD8$^+$ T cell responses were significantly immunodominant over A2/S_{269}, A24/S_{1208}, and DPB4/S_{167} (p values < 0.0036) in RBD IgG$^+$ children (Figure 2E), which was similarly observed in adults, albeit at higher frequencies.

Thus, seroconverted children had ~3.9-fold lower ORF1a- and N-specific CD8$^+$ T cell responses compared with adults but comparable Spike-specific T cell responses.

Lower Tcm-like and more Tscm SARS-CoV-2-specific CD8$^+$ T cells observed in seroconverted children compared with adults

We characterized the *ex vivo* phenotype profiles of circulating SARS-CoV-2 tetramer-specific T cells in children and adults (Figure 3A). In pooled CD8$^+$ T cell responses, RBD IgG$^+$ children had less Tcm (p = 0.0027) and more Tscm cells (p = 0.0004) than adults (Figure 3B). DPB4/S_{167}-specific CD4$^+$ T cell responses shared similar phenotypes in RBD IgG$^+$ children and adults (Figure 3B). Not surprisingly, RBD IgG$^-$ children and adults had higher Tnaive and less Tcm cells than RBD IgG$^+$ groups for pooled CD8$^+$ and CD4$^+$ T cell epitopes (Figure 3B).

Given that SARS-CoV-2-specific T cell frequencies increased with age in RBD IgG$^+$ individuals (Figure S4B), the predominance of Tcm/Tem-like tetramer$^+$ T cells in RBD IgG$^+$ individuals also significantly increased with age, whereas Tscm/naive cells decreased (Figure 3C). Similar phenotypic profiles were observed toward internal epitopes, with less Tcm-like but more Tscm/naive ORF1a- and N-specific CD8$^+$ T cells in RBD IgG$^+$ children than adults (Figure 3D). RBD IgG$^+$ children had more Tcm-like Spike-specific T cells than adults. Per epitope, we found fewer B7/N_{105}- and A3/N_{361}-specific Tcm-like cells in RBD IgG$^+$ children than in adults (p < 0.0001 and 0.0012, respectively) and more Tscm A3/N_{361}-specific T cells in children (p = 0.0003) (Figure 3E).

Thus, we provide evidence for SARS-CoV-2-specific adaptive immune responses in SARS-CoV-2 unvaccinated, seroconverted children compared with adults at convalescence. Tcm CD8$^+$ T cells were lower in children than adults, but children had increased Tscm cells following infection.

Lower SARS-CoV-2-specific T cell frequencies detected in seroconverted children compared with matched mothers

21 household families were recruited with at least one PCR$^+$ and/or RBD IgG$^+$ child, sibling, or mother to perform T cell analyses for matched children-mother samples. Enriched tetramer-specific CD8$^+$ and CD4$^+$ T cells were readily observed in RBD IgG$^+$ families compared with RBD IgG$^-$ (Figure 4A). Frequencies and numbers (per million CD4$^+$ or CD8$^+$ T cells) of SARS-CoV-2-specific T cells were similar between RBD IgG$^+$ children and mothers, but RBD IgG$^+$ children had lower mean T cell frequency (3.98 × 10^{-5}) than mothers (1.73 × 10^{-4}) (Figures 4B and 4C), reflecting those observed in the larger children-adult cohort. A1/ORF1a$_{1637}$- and/or B7/N_{105}-specific CD8$^+$ T cell responses were most immunodominant in mothers and children regardless of RBD IgG status, which resembled the immunodominance hierarchy seen in the larger cohort (Figure 2E). In households where both mothers and children expressed the dominant A1/ORF1a$_{1637}$ and/or B7/N_{105} epitope, the highest frequency was observed in mothers (RBD IgG$^+$ family 46, 78, and 102; RBD IgG$^-$ family 25, 34, and 52). This pattern was less obvious for subdominant epitopes. Mothers of RBD IgG$^+$ families (61, 78, and 88) displayed higher B40/N_{322}-, A2/S_{269}-, A24/S_{1208}-, and DPB4/S_{167}-specific T cell frequencies than children, whereas precursor frequencies in RBD IgG$^-$ households were either higher in the mother (family 18 [A2/S_{269}], 34, 52 [DPB4/S_{167}], and 53) or in children (family 18 [DPB4/S_{167}], 21, 36, 43, 52 [A2/S_{269}], 57, and 75). A3/N_{361}-specific CD8$^+$ T cell frequencies were higher in children of RBD IgG$^+$ household (family 97) and RBD IgG$^-$ household (family 36). The mothers in households 58 and 80 did not seroconvert, corresponding to lower CD4$^+$ and CD8$^+$ T cell frequencies compared with their seroconverted children (Figures 4B and 4C).

(A) Representative flow cytometry plots of enriched tetramer$^+$ T cells from RBD IgG$^+$ children and adults.
(B) Frequencies of enriched tetramer$^+$ T cells when all 7 SARS-CoV-2 epitopes were pooled with individuals grouped by RBD IgG status in children and adults or (C) by ORF1a/N or Spike epitopes.
(B and C) Statistical significance was determined with Kruskal-Wallis test.
(D) Individual frequencies per epitope from RBD IgG$^+$ or IgG$^-$ children and adults. Statistical significance was determined with Mann-Whitney U test.
(E) Hierarchy of tetramer frequencies of individual epitopes in RBD IgG$^+$ children and adults.
(B–E) Data are shown as mean with SD. 16 datasets are derived from our previous COVID-19 adult cohort (Nguyen et al., 2021b).
See also Figure S2.

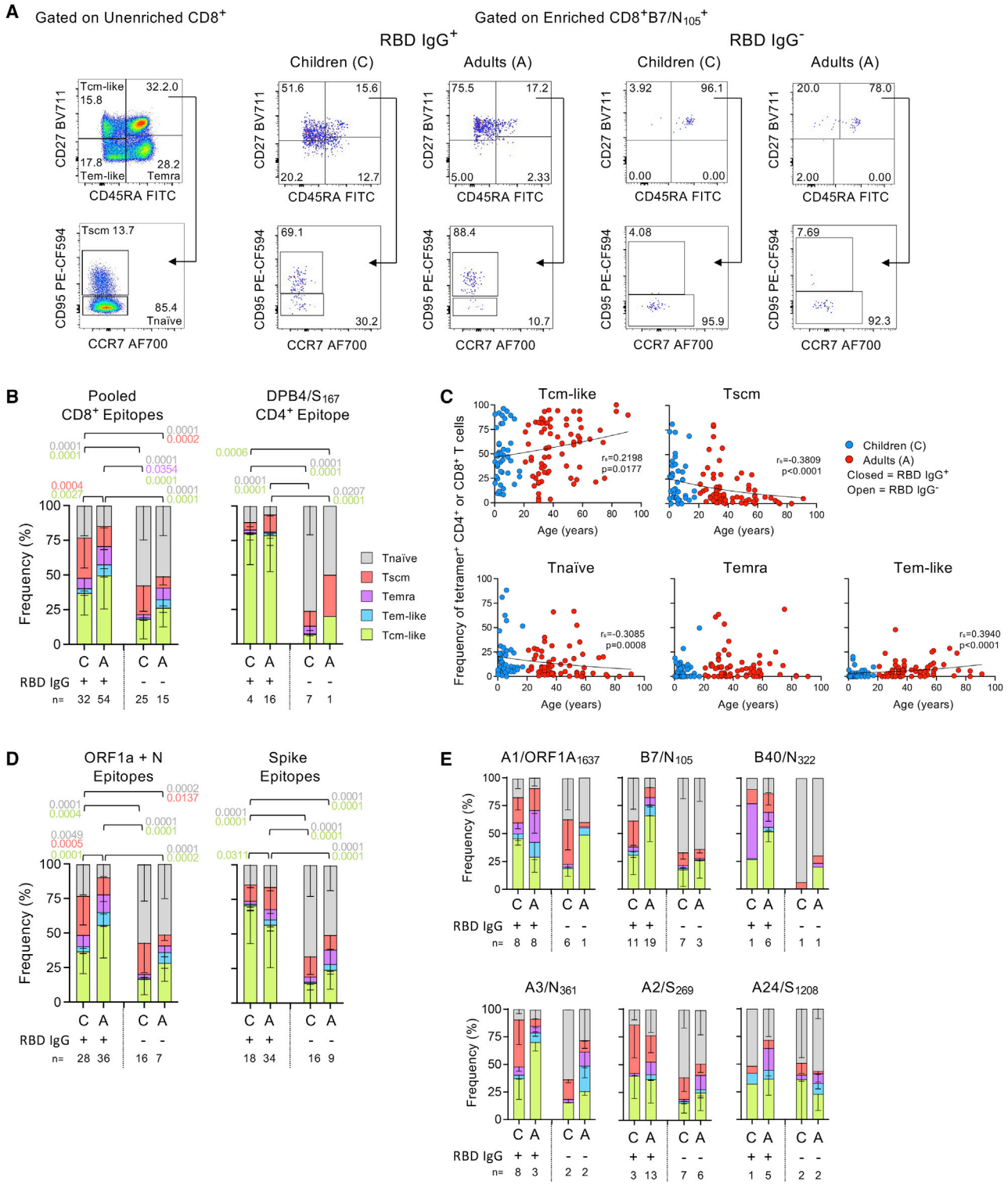

Figure 3. *Ex vivo* phenotypes of SARS-CoV-2-specific CD8$^+$ and CD4$^+$ T cells revealed in SARS-CoV-2-exposed children and adults

(A) Representative flow cytometry plots of unenriched CD8$^+$ T cells and enriched B7/N$_{105}$-specific CD8$^+$ T cells from RBD IgG$^+$ and RBD IgG$^-$ children and adults representing Tnaive-like (CD27$^+$CD45RA$^+$CD95$^-$), Tscm-like (CD27$^+$CD45RA$^+$CD95$^+$), Tcm-like (CD27$^+$CD45RA$^-$), Tem-like (CD27$^-$CD45RA$^-$), and Temra-like (CD27$^-$CD45RA$^+$) subsets. Phenotype gates were set on unenriched CD8$^+$ or CD4$^+$ T cells and applied to the enriched tetramer$^+$CD8$^+$ or CD4$^+$ T cell population.

(B) Stacked plots of phenotype subset frequency for the pooled 6 CD8$^+$ epitopes and DPB4/S$_{167}$ CD4$^+$ epitope in RBD IgG$^+$ or IgG$^-$ children and adults.

(C) Correlation of tetramer$^+$ frequencies from RBD IgG$^+$ individuals with age across the different phenotype subsets using Spearman's rank correlation (r_s).

(legend continued on next page)

SARS-CoV-2-specific T cells of household-matched RBD IgG$^+$ children (n = 14) were mainly Tcm-like (Figure 4D), except for a Tscm-dominated phenotype in selected siblings (children 46.3 and 46.4, epitopes A3/N_{361} and B7/N_{105}) or selected epitopes within children (88.2: A1/ORF1a$_{1636}$; 94.3: A2/S_{269}; 78.4: A2/S_{269} and B7/N_{105}) and Temra phenotype in 1 child (61.5: B40/N_{322}) (Figure 4B). In contrast, T cell responses in household-matched RBD IgG$^-$ children (n = 14) were mainly Tnaive, except for 2 children (18.3 and 55.4) who had Tscm phenotype toward A1/ORF1a$_{1637}$ and Tnaive phenotype for the other epitopes (Figure 4D). Similar phenotype patterns were observed among household-matched mothers, where SARS-CoV-2-specific T cell responses from RBD IgG$^+$ mothers were mainly Tcm-like but mainly Tnaive in RBD IgG$^-$ mothers (Figure 4D).

SARS-CoV-2-specific T cells in RBD IgG$^+$ children display prominent gene segment usage

TCRαβ repertoire determines the molecular signature underpinning epitope-specific T cell responses and affects T cell immunodominance, functionality, and protection (Messaoudi et al., 2002; Ndhlovu et al., 2015; Price et al., 2009; van de Sandt et al., 2019). To understand SARS-CoV-2-specific T cells at the molecular level in children, we determined TCRαβ repertoires for all 6 CD8$^+$ and 1 CD4$^+$ tetramer-specific T cell epitopes. Using direct *ex vivo* TAME and single-cell TCRαβ multiplex RT-PCR (Nguyen et al., 2018; Valkenburg et al., 2016), we dissected SARS-CoV-2-specific TCRαβ clonal composition and diversity in PBMCs from 32 children and 16 adults. This was compared with previously published TCR datasets for B7/N_{105}, A2/S_{269}, and A24/S_{1208} (Nguyen et al., 2021b; Rowntree et al., 2021b), resulting in 1,579 SARS-CoV-2-specific TCRαβ clonotypes from RBD IgG$^+$ and IgG$^-$ children and adults (Table S2).

For pooled TCRαβ repertoire analyses, variable (Vα and Vβ) and junction (Jα and Jβ) gene usage were similar between RBD IgG$^+$ children and adults (Figures 5A and 5B). Principal-component analyses (PCAs) of Vα, Vβ, Jα, and Jβ gene segments usage identified clustering segments specific to tetramer$^+$ T cells. TCRαβ clonotypes within RBD IgG$^+$ SARS-CoV-2-specific T cells closely clustered based on Vα and Vβ signatures (Figure 5A), suggesting closely related TCRαβ clonotypes, indicative of an effective epitope-specific T cell response. TCR repertoires in RBD IgG$^+$ adults had clonal expansions of Vα, Jα, Vβ, and Jβ usage, which were not seen in children. For TCR sequences identified more than once, 59.72% were from RBD IgG$^+$ adults, whereas only 34.72% were from RBD IgG$^+$ children (Table S2). However, RBD IgG$^+$ children did exhibit TRAV35/TRAJ42 clusters enriched by DPB4/S_{167}-specific CD4$^+$ T cell repertoires, as seen in RBD IgG$^+$ adults (Figure 5A). TCRαβ features within RBD IgG$^-$ individuals were more diverse and dispersed (Figure S3A), in accordance with their predominantly naive phenotype (Figure 3B).

We further dissected correlations between V and J segment usage within TCRα or TCRβ chains (Vα-Jα and Vβ-Jβ) and across TCRαβ chains (Vα-Vβ, Vα-Jβ, and Vβ-Jα). Repertoires in RBD IgG$^+$ children and adults were biased and had 6-fold enrichment of TRAV35, with the majority joined to TRAJ42 (children: 6-fold; adults: 4-fold enrichment) and paired with 2-fold enrichment to TRBJ1-2 (children) or TRBJ2-1 (adults), which joined a range of different TRBV genes, mainly attributable to the DPB4/S_{167}-specific CD4$^+$ TCR repertoire (Figure 5B). TRBV27 was the most frequent Vβ gene segment (2-fold enrichment) in RBD IgG$^+$ cohorts; however, this gene paired with different TRBJ, TRAV, and TRAJ segments, with the resulting TCRs restricted to several different epitopes (Figures 5B, 5C, and S3C). TCRαβ repertoires identified in RBD IgG$^+$ children were comparable with repertoires identified in RBD IgG$^+$ adults, with similar V and J segment usage. Conversely, there was a high degree of TCRαβ repertoire diversity in RBD IgG$^-$ children and adults (Figure S3B), especially within the pairing of TCRα and TCRβ gene segments, consistent with their naive T cell phenotype (Figure 3B).

To determine the overall TCRαβ diversity within each epitope between RBD IgG$^+$ children and adults, circos and bubble plots revealed that SARS-CoV-2-specific TCRαβ repertoires were quite diverse, with an average of 14 and 16 TCRαβ clonotypes per donor/epitope in children and adults, respectively (Figures 5C, 5D, S3C, and S4). In contrast, RBD IgG$^-$ children and adults had an average of 9 TCRαβ clonotypes each (Table S2). RBD IgG$^+$ children and adults displayed a skewed bias for selected TRAV and/or TRBV gene segments. For example, the B7/N_{105}-, A1/ORF1a$_{1637}$-, and B40/N_{322}-specific repertoires had enrichments for TRBV27 gene usage in RBD IgG$^+$ children and adults compared with RBD IgG$^-$ individuals (Figures 5C, 5D, and S3C; Table S2). In line with the previous report (Mudd et al., 2022), DPB4/S_{167}-specific CD4$^+$ T cells displayed a heavy bias for TRAV35/TRAJ42 gene segments, which accounted for the majority of the TCRα repertoire in RBD IgG$^+$ children and adults (80.77% and 76.25%, respectively) but to a lesser extent in RBD IgG$^-$ children and adults (50.00% and 40.00%, respectively). These TRAV35/TRAJ42 clonotypes commonly paired with TRBVs 6-1, 6-2/3, 6-5, 6-6, 9, and 27, which were observed among both RBD IgG$^+$ children and adults, suggesting common TCRαβ repertoire features between children and adults for DPB4/S_{167}-specific CD4$^+$ T cells (Figures 5C and 5D; Table S2).

Within several epitopes, CDR3α or CDR3β chains were shared between multiple individuals (n = 2–17) (Table S3). The shared CDR3α chains were detected for A1/ORF1a$_{1637}^+$ (TRAV9-2/TRAJ42 CALGGSQGNLIF), A2/S_{269}^+ (TRAV12-2/TRAJ30 CAVNRDDKIIF and TRAV12-1/TRAJ43 CVVNKGNDMRF/CVVNNNNDMRF/CVVNRNNDMRF), and B7/N_{105}^+ CD8$^+$ TCR repertoires (TRAV8-2/8-4 with TRAJ48 CAVPNFGNEKLTF or TRAJ3 CAVPSYSSASKIIF). The shared CDR3β chains were observed for A2/S_{269}^+ (TRBV7-9 with TRBJ2-2 CASGEGNTGELFF or TRBJ2-7 CASSLDIEQYF), B7/N_{105}^+ (TRBV27/TRBJ1-5 CASSLSYRGNQPQHF, TRBV27/TRBJ1-1 CASSLSYRGNTEAFF, and TRBV2/TRBJ1-1 CASSEKTGGSTEAFF), and B40/N_{322}^+ CD8$^+$ T cells (TRBV27/TRBJ1-4 CASSFSNEKLFF) (Table S3). This was particularly observed in the DPB4/S_{167}-specific CD4$^+$ TCR repertoire, where 16 diverse albeit prominent TRAV35/TRAJ42$^+$ CDR3α

(D) Stacked phenotype plots based on ORF1a/N (A1/ORF1a$_{1637}$, A3/N_{361}, B7/N_{105}, and B40/N_{322}) and Spike epitopes (A2/S_{269}, A24/S_{1208}, and DPB4/S_{167}) or (E) per individual CD8$^+$ epitope. Only individuals above the detection limit ($\geq$10 tetramer$^+$-enriched events) were included for analysis.
(B, D, and E) Mean with SD is shown, and statistical significance was determined using Tukey's multiple comparisons test.

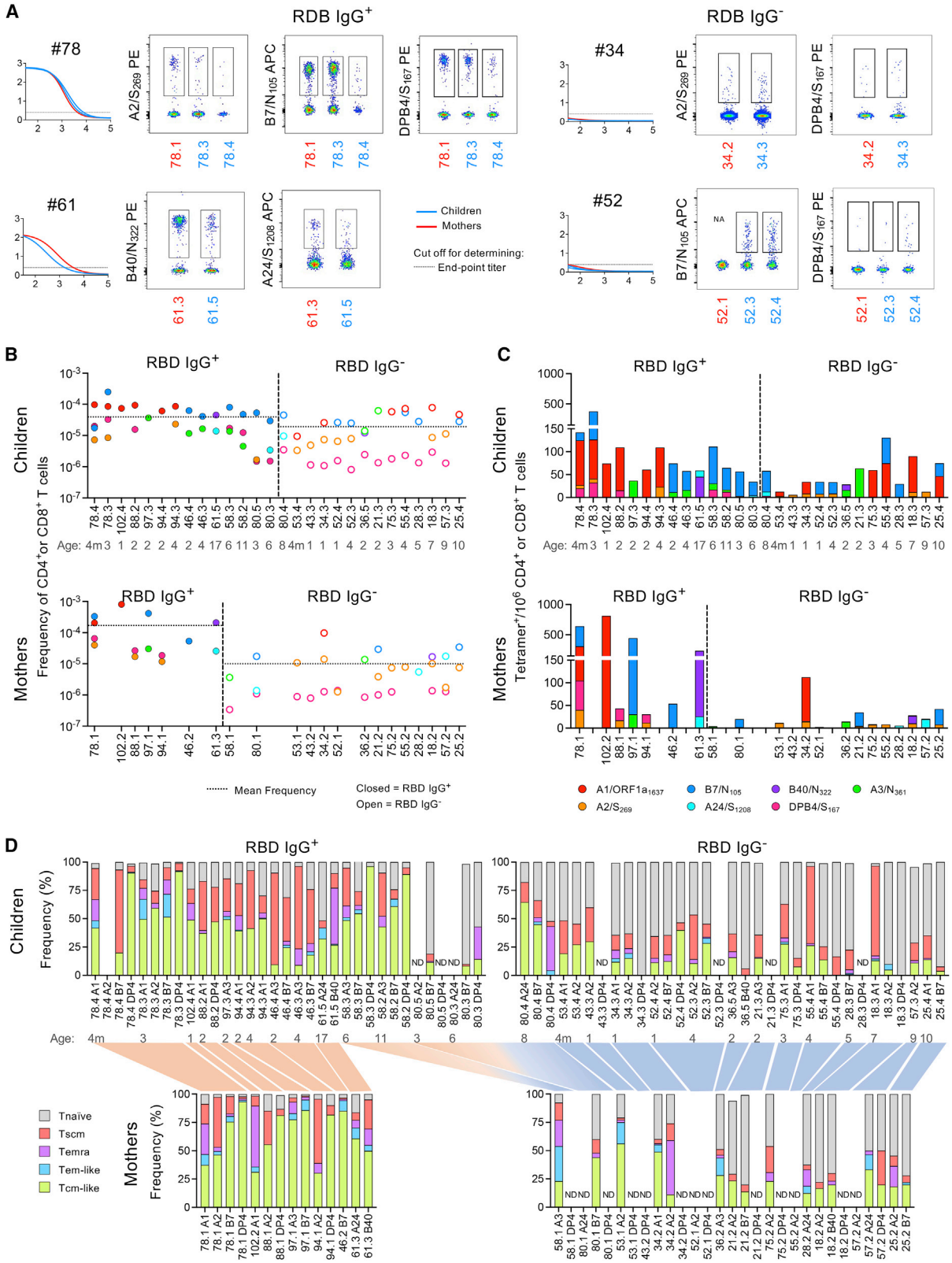

Figure 4. SARS-CoV-2-specific CD8⁺ and CD4⁺ T cells profiled in children and mothers

(A) Representative flow cytometry plots of enriched tetramer⁺ T cells from families with RBD IgG⁺ or RBD IgG⁻ children, as depicted by RBD IgG dilution curves. (B and C) Individual participant profiles of SARS-CoV-2 epitope-specific T cell (B) frequencies and (C) cumulative tetramer⁺ cells per million CD4⁺ or CD8⁺ T cells.

(legend continued on next page)

chains (paired with a range of CDR3β chains) were observed in 22/31 individuals tested. Common CDR3 sequences were identified across repertoires of at least 2 individuals, but each participant used different variable gene segments. For instance, A1/ORF1a$_{1637}$'s CDR3α CALNTGNQFYF was generated via arrangements of TRAV9-2 or TRAV29/DV5, whereas A2/S$_{269}$'s CDR3β CASSLGGNQPQHF was generated by TRBV13 or TRBV27, and DPB4/S$_{167}$'s CDR3β CASSLRGDYGYTF was produced by TRBV11-2 or TRBV6-2/6-3, suggesting that these CDR3β-loops are preferentially selected in the general population post-COVID-19 (Table S3).

Analyses of SARS-CoV-2-specific CD8$^+$ and CD4$^+$ T cells revealed skewed biases for TRAV and/or TRBV gene segments in RBD IgG$^+$ children and adults, with RBD IgG$^+$ adults displaying expansions across different gene segments that were not observed in RBD IgG$^+$ children. Meanwhile, highly diverse TRAV and/or TRBV gene segment usage featured in RBD IgG$^-$ individuals.

Enriched SARS-CoV-2-specific TCRαβ motifs observed in RBD IgG$^+$ children and adults

The preferential recombination of CDR3-loops was further investigated by analyses of TCR motifs with similar or near-identical CDR3 regions within each TCRα or TCRβ chain in RBD IgG$^+$ individuals. This was quantified by a neighbor distance distribution plot, where lower average values of the distance distribution peak represented a more similar clustering of clonotypes (Figures 6A and S5A). Distribution of A2/S$_{269}$-specific TCRαβ sequences differed between RBD IgG$^+$ children and adults, mainly driven by an approximately bimodal distribution in the adult TCRα chain compared with a single peak distribution in children (children: α = 119.5, β = 96.3, αβ = 245.5; adults: α = 76.0, β = 75.3, αβ = 169.4 average distance value). In contrast, differences in A24/S$_{1208}$ TCRαβ repertoire distribution were driven by the TCRβ chain, with children displaying a lower distance distribution than adults (children: α = 146.0, β = 80.5, αβ = 237.9; adults: α = 118.6, β = 137.6, αβ = 269.9). DPB4/S$_{167}$-specific CD4$^+$ TCRαβ sequences in both RBD IgG$^+$ children and adults had the lowest distance distribution, with clustering driven by the TCRα chain (children: α = 10.6, β = 91.9, αβ = 109.3; adults: α = 13.7, β = 90.5, αβ = 112.5) (Figure 6A). Conversely, DPB4/S$_{167}$-specific CD4$^+$ TCRαβ sequences from RBD IgG$^-$ individuals clustered into 2 peaks, the lower peak for the conserved TCRα chain and the higher peak for the more diverse TCRβ chain (children: α = 56.2, β = 112.8, αβ = 185.2; adults: α = 63.4, β = 115.8, αβ = 201.0) (Figure S5A).

TCRαβ sequences for each epitope were analyzed for key motifs within children and adults, with more TCRα and β motifs identified in adults than children (Figure 6B). Motifs were highly enriched and more prevalent in RBD IgG$^+$ individuals (children: 1xα, 6xβ; adults 4xα, 8xβ), with only 1 weak motif identified in RBD IgG$^-$ adults (1xβ, chi-squared 90.2) (Figure S5B). The only prominent TCRα motif identified in children and adults was for DPB4/S$_{167}$ dataset (TRAV35/TRAJ42 chi-squared children: 1,733.2, adults: 637.1), while TCRα motifs were also identified for A1/ORF1a$_{1637}$-, B7/N$_{105}$-, and A2/S$_{269}$-specific TCRs in the RBD IgG$^+$ adults (Figure 6B). Prominent TCRβ motifs for DPB4/S$_{167}$ were identified in children (4xβ, chi-squared between 380.8 and 2,070.2) and adults (3xβ, chi-squared between 212.9–380.2), with multiple motifs sharing TRBJ1-2 usage and "CASSXRG" CDR3β-loop. Similar A1/ORF1a$_{1637}$ TCRβ motifs were identified in children and adults (TRBV27/TRBJ2-2 children: 306.2, adults: 161.3), while the B7/N$_{105}$-specific motif was more varied between cohorts (children: TRBV27 chi-squared 462.2; adults: TRBV25 chi-squared 462.2 and TRBV27 chi-squared 306.2), and the A2/S$_{269}$-specific motifs were only identified in adults.

The probability of generating (P$_{gen}$) TCRα or TCRβ chains was calculated for each epitope (Figure 6C). Within the TCRα chain, the probability of generating α-chains specific for the DPB4/S$_{167}$$^+$CD4$^+$ epitope in RBD IgG$^+$ children and adults was increased compared with the P$_{gen}$ values across the 6 SARS-CoV-2 CD8$^+$ T cell epitopes. Conversely, the probability for recombination of the TCRβ chain specific to the DPB4/S$_{167}$$^+$CD4$^+$ epitope was comparable with the CD8$^+$ epitopes, particularly A1/ORF1a$_{1637}$, A3/N$_{361}$, and B7/N$_{105}$. This lower P$_{gen}$ for the TCRβ chain reflects an increased diversity in the TCRβ repertoire and suggests that any enrichment or skewed bias of particular motifs did not result from fewer constraints for recombination.

Overall, our data on high frequency, Tcm phenotype, and prominent TCRαβ motifs within SARS-CoV-2-specific T cells in seroconverted COVID-19 children suggest recruitment of T cell responses following SARS-CoV-2 infection and the subsequent establishment of memory T cell pools.

DISCUSSION

The gradual opening of society due to the mass vaccination of adults and the elderly together with the rapid spread of the SARS-CoV-2 Omicron variant has increased the risk of COVID-19 in children (Delahoy et al., 2021; Mallapaty, 2021). Despite COVID-19 vaccination approval for children aged 5 and over in most countries, vaccination rates in children globally are lagging. Thus, it is of key importance to understand immunological responses to SARS-CoV-2 infection in unvaccinated children and their potential to establish immunological memory. Our study provides in-depth *ex vivo* profiling of circulating SARS-CoV-2-specific epitope-specific T and B cell immunity in children and adults. Our findings revealed lower ORF1a- and N-specific cellular responses in seroconverted convalescent children compared with adults. Spike-specific B cell responses were observed in seroconverted children and adults. Exposed seronegative children had naive T cells and diverse TCRαβ repertoires.

The lack of adaptive immunity in some children can be related to stronger early antiviral innate and mucosal immune response to SARS-CoV-2, likely contributing to rapid viral clearance and potentially explaining milder disease outcomes (Loske et al., 2022; Neeland et al., 2021a, 2021b; Pierce et al., 2020; Toh et al., 2022; Tosif et al., 2020). Alternatively, those seronegative children may have been exposed to a lower viral load, insufficient to induce adaptive immune responses. Reduced immune responses and lack of bystander T cell activation, resulting in

(D) Stacked plots display the proportion of each phenotype subset within epitope-specific T cell responses for each individual. The families are linked between the children and mothers by red (RBD IgG$^+$) or blue (RBD IgG$^-$) shading. The x axis depicts the participant and HLA restriction of the epitope examined; A1/ORF1a$_{1637}$, A2/S$_{269}$, A3/N$_{361}$, A24/S$_{1208}$, B7/N$_{105}$, B40/N$_{322}$ and DPB4/S$_{167}$.

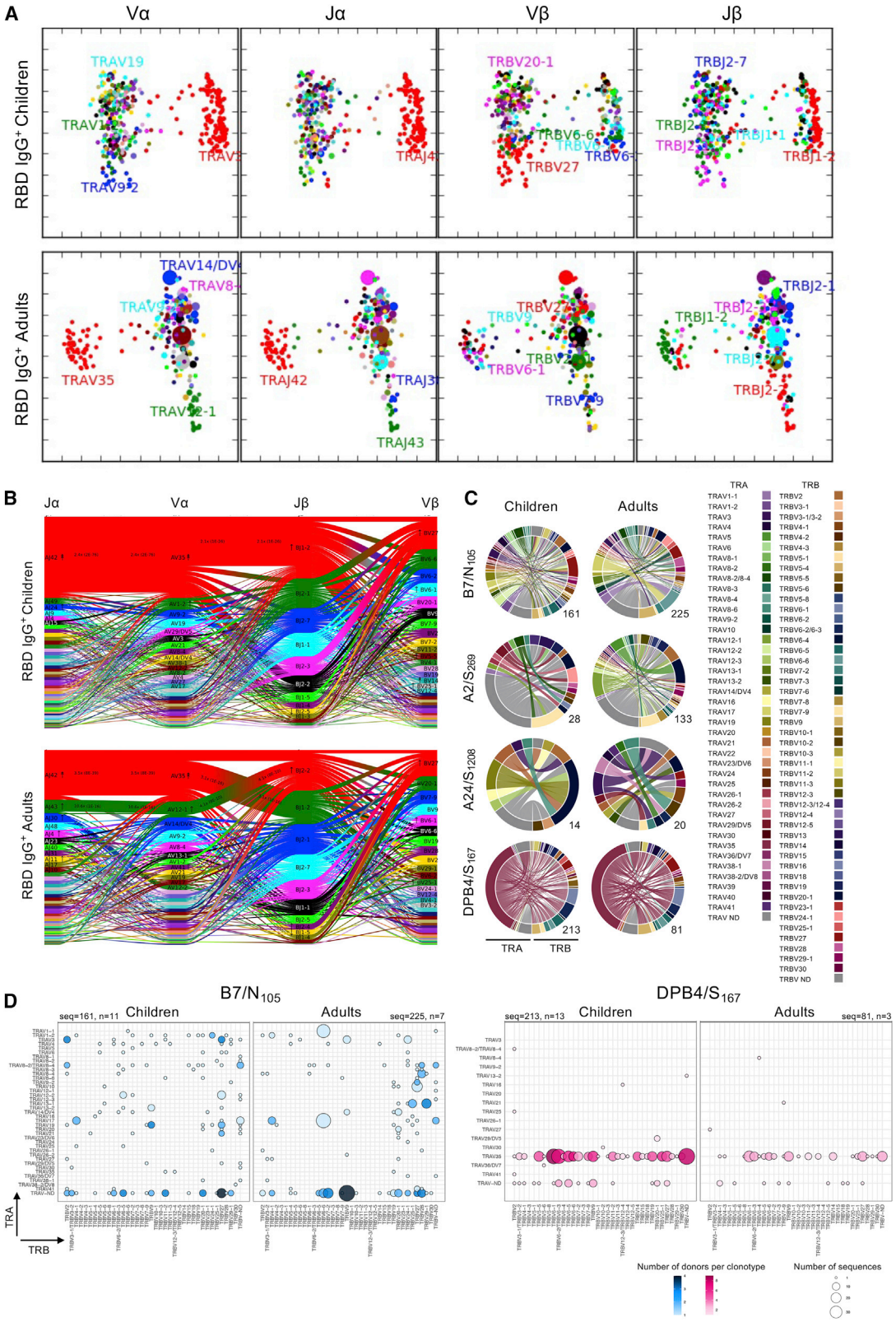

(legend on next page)

less immunopathology and thus milder disease in children, has also been suggested (Brodin, 2022).

Prior to our study, the *ex vivo* epitope-specific $CD8^+$ and $CD4^+$ T cell responses following natural SARS-CoV-2 infection of children were ill-defined. Our in-depth quantitative, phenotypic, and clonal profiling of *ex vivo* epitope-specific T cell responses found that seroconverted, unvaccinated children had memory SARS-CoV-2-specific T cell profiles across 7 HLA class I and II SARS-CoV-2 epitopes and S-specific B cells. Lower SARS-CoV-2 $tetramer^+$ T cell frequency and the proportion of $CD8^+$ Tcm cells were observed in seroconverted children compared with adults, while the frequency of SARS-CoV-2-specific $CD8^+$ Tscm cells was increased in children. Reduced $CD4^+$ and $CD8^+$ T cell responses in children with mild COVID-19 compared with adults were also observed following overlapping SARS-CoV-2 peptide pool stimulation (Cohen et al., 2021; Goenka et al., 2021; Moratto et al., 2020; Pierce et al., 2020). Diminished IFN-γ-producing cellular responses to N- and M-derived peptides and 2-fold increased responses to S-derived peptides were previously observed (Dowell et al., 2022). Our unbiased *ex vivo* analysis demonstrates a higher magnitude of tetramer-specific T cells directed at epitopes encompassing peptides derived from N ($A3/N_{361}$, $B7/N_{105}$, and $B40/N_{322}$) and ORF1a ($A1/ORF1a_{1637}$) compared with S-derived peptides ($A2/S_{269}$, $A24/S_{1208}$, and $DPB4/S_{167}$) in both children and adults and a ~3.9-fold lower frequency of internal protein-specific $CD8^+$ T cells in children compared with adults, which was reflected by their immunodominance hierarchy. Differential peptide-stimulated T cell responses between children and adults could also, at least in part, reflect differences in antigen presentation and/or functionality of T cells.

Seroconverted children and adults displayed strong memory phenotypes of circulating SARS-CoV-2-specific $CD8^+$ and $CD4^+$ T cells. $Tetramer^+CD8^+$ T cells from seroconverted children had a reduced Tcm but increased Tscm phenotype compared with adults, while there was no difference in the $CD4^+$ $DPB4/S_{167}$-specific phenotypic profiles. Previous studies using *in vitro* peptide stimulation and IFN-γ readout showed reduced Tem phenotype within $CD4^+$ T cells, with a substantially increased Tcm phenotype in children compared with adults (Cohen et al., 2021).

Our TCR$\alpha\beta$ analysis revealed closely related TCR$\alpha\beta$ clonotypes, with prominent SARS-CoV-2-specific TCR gene segments and motifs, within SARS-CoV-2-specific T cells in RBD IgG^+ children and adults cluster according to their Vα, Vβ, Jα, and Jβ signatures, indicating selective recruitment of epitope-specific T cells following SARS-CoV-2 infection. These findings agree with studies that reported a biased TRAV and TRBV gene usage and prevalent motifs in adults during COVID-19 (Francis et al., 2022; Gangaev et al., 2021; Minervina et al., 2022; Nguyen et al., 2021b; Rowntree et al., 2021b; Shomuradova et al., 2020). Prior to our study, *ex vivo* epitope-specific TCR analysis in mildly infected children was non-existent. Bulk TCR analysis in MIS-C patients reported enrichment of TRBV11-2 in both the $CD8^+$ and $CD4^+$ TCR repertoire (Moreews et al., 2021; Porritt et al., 2021; Ramaswamy et al., 2021). Although we identified T cells expressing TRBV11-2 in our cohort, these were not expanded or enriched in mildly infected children. TRBV11-2 enrichment in MIS-C children may be specific for a different epitope or, as claimed by the authors, TRBV11-2 may bind a superantigen (SAg)-like motif on the S1 trimer in a HLA-independent manner (Porritt et al., 2021). However, it is unknown whether repeated SARS-CoV-2 infections and/or vaccinations in children and adults will skew the TCR repertoire in favor of certain epitopes or clonotypes.

Conversely, circulating tetramer-specific $CD4^+$ and $CD8^+$ T cells in exposed, seronegative children and adults displayed lower frequencies and a naive T cell phenotype, in accordance with their overall more diverse and unbiased TCR$\alpha\beta$ repertoire observed across all T cell epitopes. Innate immune responses in a small subgroup of PCR^+ seronegative children may have cleared the SARS-CoV-2 infection prior to eliciting circulating adaptive immunity, as evidenced by low frequencies of predominantly naive $tetramer^+$ $CD4^+$ and $CD8^+$ T cells (Neeland et al., 2021a; Neeland et al., 2021b). This may also explain the observed diminished overlapping SARS-CoV-2 peptide pool stimulated $CD4^+$ and $CD8^+$ T cell response in SARS-CoV-2-infected children reported by others (Cohen et al., 2021; Goenka et al., 2021; Moratto et al., 2020; Pierce et al., 2020). Furthermore, we only defined circulating memory SARS-CoV-2-specific $CD8^+$ and $CD4^+$ T cells using children's PBMCs, whereas a recent report identified cross-reactive $CD8^+$ T cells in children only in the lymphoid tissue but not in blood (Niessl et al., 2021).

Figure 5. SARS-CoV-2-specific TCR$\alpha\beta$ repertoires are comparable between children and adults

SARS-CoV-2-specific $CD4^+$ and $CD8^+$ T cells were enriched by TAME and then single-cell sorted for TCR$\alpha\beta$ analysis.

(A) TCR landscapes displayed using kernel PCA projections of pooled SARS-CoV-2-specific TCRs were generated by TCRdist for all TCR$\alpha\beta$ pairs. Vα, Jα, Vβ, and Jβ usage are depicted for RBD IgG^+ children and adults. Encoding clone size is indicated by the symbol size.

(B) V and J gene segment usage and covariation in SARS-CoV-2-specific responses. Gene segment usage is shown in vertical stacks, with gene-gene pairing landscapes depicted by curved segments (thickness proportional to the number of TCRs with the gene pairing). Up or down arrows indicate the enrichment of gene segments relative to background frequencies, with each arrowhead indicating a 2-fold enrichment. The clonally expanded TCRs were reduced to a single data point for this analysis.

(A and B) Genes are colored based on frequency: red (most frequent), green (second most frequent), blue, cyan, magenta, and black, followed by assorted colors for rare frequencies.

(C) Circos plots of TRAV and TRBV clonotype pairings for $B7/N_{105}$, $A2/S_{269}$, $A24/S_{1208}$, and $DPB4/S_{167}$ epitopes in the RBD IgG^+ children and adults; left arch and segment color indicate TRAV usage, and the right outer arch color depicts TRBV usage. The segments shown by the same color represent TCR$\alpha\beta$ clonotypes with the same V segment usage but different CDR3 sequences. The number of sequences considered for each Circos plot is shown at the bottom right.

(D) Bubble plot showing the distribution (number of donors and frequency) of TRBV/TRAV gene usage for $B7/N_{105}$ and $DPB4/S_{167}$ epitopes in RBD IgG^+ children and adults. Previously published adult TCR datasets for $B7/N_{105}$, $A2/S_{269}$, and $A24/S_{1208}$ were included in the adult TCR analysis (Nguyen et al., 2021b; Rowntree et al., 2021b).

See also Figures S3 and S4.

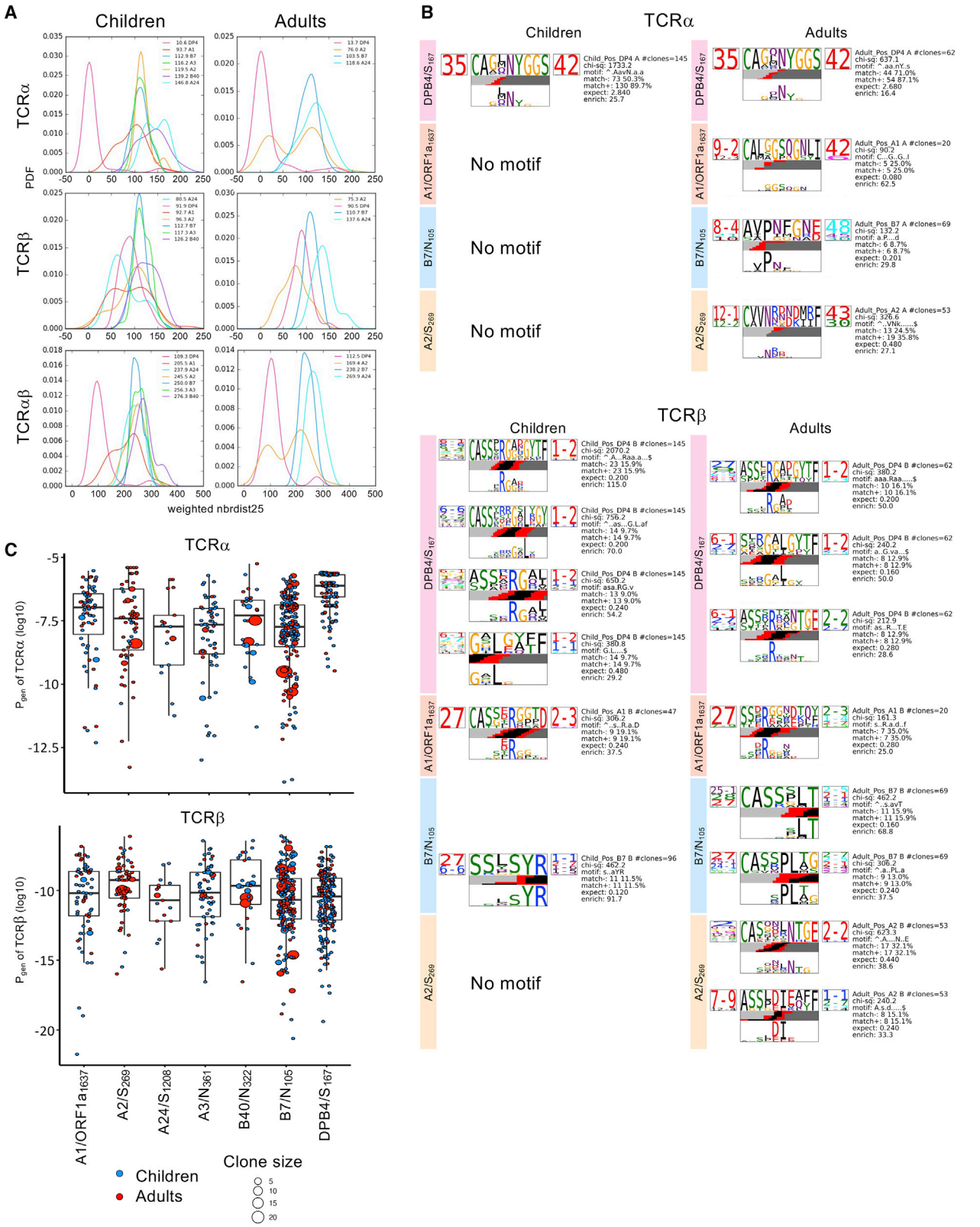

(legend on next page)

Hence, there is a possibility that adaptive immune responses in the lymphoid tissue of these children was undetectable in the blood. However, our study used a sensitive tetramer enrichment technique to identify low-frequency SARS-CoV-2-specific $CD8^+$ and $CD4^+$ T cell populations. Even if transient SARS-CoV-2-specific T cell responses were only present early following SARS-CoV-2 infection, the detected $tetramer^+$ T cells had a predominantly naive phenotype within the circulating T cell compartment in seronegative, exposed children. In contrast, SARS-CoV-2-specific Tcm and Tscm phenotypes were identified in seroconverted children.

We may have missed the window of opportunity for PCR testing in some families, like in seroconverted PCR-negative family 78 that had a clear SARS-CoV-2-specific T cell memory response, which is in accordance with previous studies that demonstrated high frequencies of predominantly memory A2/S_{269}^+, A24/S_{1208}^+, and B7/N_{105}^+ $CD8^+$ T cells in convalescent SARS-CoV-2 PCR confirmed adults (Chaurasia et al., 2021; Habel et al., 2020; Nguyen et al., 2021b; Rowntree et al., 2021b). However, the exposed, PCR^-, seronegative children and mainly adults from our cohort displayed low T cell frequencies and naive phenotypes, which closely resembled those of pre-pandemic adults, and were therefore likely not infected with SARS-CoV-2 (Francis et al., 2022; Gangaev et al., 2021; Habel et al., 2020; Nguyen et al., 2021b; Rowntree et al., 2021b). In addition, children are less likely to spread the virus to adult family members in a household setting (Zhu et al., 2021). Finally, the small subgroup of PCR^+ seronegative children indicates that rapid viral clearance may have precluded a select group of children from generating adaptive immunological memory. As our number of PCR^+, seronegative children is small (n = 11), our data should be verified in a larger cohort.

Our study provides clear evidence that children who seroconvert established memory $CD8^+$ and $CD4^+$ T cell responses to SARS-CoV-2 epitopes, which are highly conserved across VOC, including the Delta and Omicron, which together with their cross-reactive antibody response can likely protect them from severe COVID-19 when exposed to new variants. It is currently uncertain whether children who failed to seroconvert during their first SARS-CoV-2 infection can also benefit from rapid antiviral innate immunity when they encounter new VOC, including the Omicron strain. Hence, our study makes a case for why vaccination of children should be considered a major advantage, as these vaccines specifically aim to induce adaptive B and T cell memory responses in all children (Collier et al., 2021; Mudd et al., 2022; Oberhardt et al., 2021; Sahin et al., 2021). Future work understanding adaptive immune memory responses in COVID-19 vaccinated children will provide important insights into whether SARS-CoV-2-specific T cell (and B cell) responses induced by vaccination differ from those following SARS-CoV-2 infection.

Limitations of the study

Our COVID-19 patients originate from two countries (Australia and the USA) and thus do not represent the global population. In our study of 53 children, 37 were SARS-CoV-2 PCR^+ of which 21% failed to seroconvert. Ct values could not be compared across cohorts, as SARS-CoV-2 PCR testing was performed across different locations, on different platforms, and for different antigens. As previously described (Toh et al., 2022), the majority of samples were tested using the LightMix Modular SARS and Wuhan CoV E-gene kit (Procop et al., 2021; TIB Molbiol, Berlin, Germany) with the RT-PCR performed on the LightCycler 480 II Real-Time PCR System (Roche). A subset of the Melbourne samples (family 102 and 104) was tested using an Allplex SARS-CoV-2 assay (Seegene), which has 4 gene targets, E, RDRP/S, and N. Los Angeles samples were tested using the CDC protocol for RT-PCR (Procop et al., 2021), which targets the SARS-CoV-2 N1/N2 genes, and the RT-PCR was performed on QuantStudio 5 (Applied Biosystems, Carlsbad, CA). Ct values were not available for the adult cohort.

STAR★METHODS

Detailed methods are provided in the online version of this paper and include the following:

- KEY RESOURCES TABLE
- RESOURCE AVAILABILITY
  - Lead contact
  - Materials availability
  - Data and code availability
- EXPERIMENTAL MODEL AND SUBJECT DETAILS
- METHOD DETAILS
  - SARS-CoV-2-specific antibodies and B cells
  - SARS-CoV-2 $tetramer^+$ T cell responses
- QUANTIFICATION AND STATISTICAL ANALYSIS
  - TCRαβ statistical analysis
  - Amino acid sequence identity
  - Statistical analysis

SUPPLEMENTAL INFORMATION

Supplemental information can be found online at https://doi.org/10.1016/j.immuni.2022.06.003.

Figure 6. RBD IgG^+ children and adults have prominent TCRαβ motifs

(A) Epitope-specific populations from RBD IgG^+ children and adults were quantified for defining features using a neighbor distance distribution. A lower distribution peak indicates a more clustered epitope-specific TCRαβ repertoire, and the average distance values for each epitope are depicted within the plot. Analyses for both single and paired chains are shown, as indicated in the plot labels. PDF, probability density function.

(B) TCR logo representations of CDR3α and β sequence motifs for RBD IgG^+ children and adults. Each TCR chain motif depicts the V (left side) and J (right side) gene frequencies, the CDR3 amino acid sequence (middle), and the inferred rearrangement structure (bottom bars colored by source region; V-region, light gray; insertions, red; diversity (D)-region, black; and J-region dark gray). The motif scores were determined by chi-squared, with values greater than 90 considered highly significant.

(C) Probabilities of generation (P_{gen}; $\log_{10}$ transformed) for all single TCRα and TCRβ chains from RBD IgG^+ children and adults were generated with TCRdist. Box plots represent the median (middle bar), 75% quantile (upper hinge), and 25% quantile (lower hinge), with whiskers extending 1.5 times the inter-quartile range. See also Figure S5.

ACKNOWLEDGMENTS

We thank the participating families involved in the study and Kate Dohle, Jill Nguyen, Isabella Overmars, Philip Sutton, and Daniel Pellicci for their support with the cohorts. We thank the Melbourne Cytometry Platform for the technical assistance. This work was supported by the NHMRC Leadership Investigator Grant to K.K. (1173871); the NHMRC Emerging Leadership Level 1 Investigator Grant to T.H.O.N. (#1194036) and A.K.W. (#1173433); the Research Grants Council of the Hong Kong Special Administrative Region, China (#T11-712/19-N) to K.K.; the Doherty Collaborative Seed grant to M.R.N., A.K.W., S.J.K., S.T., C.E.v.d.S., and K.K.; the Victorian Government (S.J.K. and A.K.W.); the Clifford Craig Foundation Project Grant to K.L.F. and K.K. (#186); the MRFF award (#2002073) to S.J.K. and A.K.W.; the MRFF Award (#1202445) to K.K.; the MRFF Award (#2005544) to K.K., S.J.K., and A.K.W.; the NHMRC program grant 1149990 (S.J.K.); the NHMRC project grant 1162760 (A.K.W.); the NIH contract CIVC-HRP (HHS-NIH-NIAID-BAA2018) to P.G.T. and K.K.; and the NIAID UO1 grant 1U01AI144616-01 "Dissection of Influenza Vaccination and Infection for Childhood Immunity" (DIVINCI) to F.K., P.G.T., K.K., and P.S.P. S.J.K. is supported by the NHMRC Senior Principal Research Fellowship (#1136322). C.E.v.d.S. received funding from the European Union's Horizon 2020 research program under the Marie Skłodowska-Curie grant agreement (#792532) and is supported by the ARC-DECRA Fellowship (#DE200100185) and University of Melbourne Establishment grant. J.R. is supported by an ARC Laureate Fellowship. J.C.C. and P.G.T. are supported by the NIH NIAID R01 AI136514-03 and the ALSAC at St. Jude. P.V.L. is supported by an NHMRC Career Development Fellowship. Work in the F.K. laboratory was partially funded by the Centers of Excellence for Influenza Research and Surveillance (CEIRS, #HHSN272201400008C), the Centers of Excellence for Influenza Research and Response (CEIRR, #75N93021C00014), by the Collaborative Influenza Vaccine Innovation Centers (CIVICs, #75N93019C00051), and by institutional funds. We acknowledge the RCH Foundation for their support of the study and recruitment of the families involved. Recruitment of the household contacts was enable by COVID-19 Grant, Department of Jobs, Precincts and Regions, Victoria State Government and Research Grant, DHB Foundation, Australia. The graphical abstract was created with BioRender.com.

AUTHOR CONTRIBUTIONS

K.K. led the study. K.K. and C.E.v.d.S. supervised the study. L.C.R., T.H.O.N., L.K., C.E.v.d.S., and K.K. designed the experiments. L.C.R., T.H.O.N., L.K., L.F.A., E.B.C., X.J., and H.-X.T. performed and analyzed the experiments. E.B.C. and H.A.M. analyzed the data. J.P., A.A.M., M.V.P., P.C., A.K.W., F.A., F.K., S.J.K., and J.R. provided the crucial reagents. M.R.N., E.K.A., S.S., K.L.F., J.J., P.S.P., P.V.L., K.A.B., D.A.W., P.G.T., S.T., and N.W.C. recruited the patient cohorts. L.C.R., T.H.O.N., J.C.C., L.F.A., H.A.M., P.G.T., and C.E.v.d.S. analyzed the TCR sequences. L.C.R., T.H.O.N., L.K., P.G.T., S.T., C.E.v.d.S., and K.K. provided the intellectual input into the study design and data interpretation. L.C.R., T.H.O.N., C.E.v.d.S., and K.K. wrote the manuscript. All authors reviewed and approved the manuscript.

DECLARATION OF INTERESTS

SARS-CoV-2 serological assays (US Provisional Application #62/994252, 63/018457, 63/020503, and 63/024436) and NDV-based SARS-CoV-2 vaccines (US Provisional Application #63/251020) list F.K. as a co-inventor. F.A. is also a co-inventor of the serological assay patents. Patent applications were submitted by the Icahn School of Medicine at Mount Sinai. Mount Sinai has spun out a company, Kantaro, to market serological tests for SARS-CoV-2. F.K. has consulted for Merck and Pfizer (before 2020) and is currently consulting for Pfizer, Third Rock Ventures, Seqirus, and Avimex. F.K. laboratory collaborates with Pfizer on the animal models of SARS-CoV-2. P.G.T. is on the SAB of Immunoscape and Cytoagents, has consulted for JNJ, received travel support and/or honoraria from Illumina, 10X Genomics, and has patents on TCR discovery and expression. P.S.P. received research grants from Astra Zeneca and Pfizer and has served on advisory boards for Sanofi Pasteur and Seqirus.

Received: October 29, 2021
Revised: March 31, 2022
Accepted: June 1, 2022
Published: June 8, 2022

REFERENCES

Amanat, F., Stadlbauer, D., Strohmeier, S., Nguyen, T.H.O., Chromikova, V., McMahon, M., Jiang, K., Arunkumar, G.A., Jurczyszak, D., Polanco, J., et al. (2020). A serological assay to detect SARS-CoV-2 seroconversion in humans. Nat. Med. *26*, 1033–1036. https://doi.org/10.1038/s41591-020-0913-5.

Bates, D., Mächler, M., Bolker, B., and Walker, S. (2014). Fitting linear mixed-effects models using lme4. J. Stat. Software *67*, 61. https://doi.org/10.18637/jss.v067.i01.

Brodin, P. (2022). SARS-CoV-2 infections in children: understanding diverse outcomes. Immunity *55*, 201–209. https://doi.org/10.1016/j.immuni.2022.01.014.

CDC COVID-19 Response Team (2020). Severe outcomes among patients with coronavirus Disease 2019 (COVID-19) - United States, February 12–March 16, 2020. MMWR Morb. Mortal. Wkly. Rep. *69*, 343–346. https://doi.org/10.15585/mmwr.mm6912e2.

Chaurasia, P., Nguyen, T.H.O., Rowntree, L.C., Juno, J.A., Wheatley, A.K., Kent, S.J., Kedzierska, K., Rossjohn, J., and Petersen, J. (2021). Structural basis of biased T cell receptor recognition of an immunodominant HLA-A2 epitope of the SARS-CoV-2 spike protein. J. Biol. Chem. *297*, 101065. https://doi.org/10.1016/j.jbc.2021.101065.

Chou, J., Thomas, P.G., and Randolph, A.G. (2022). Immunology of SARS-CoV-2 infection in children. Nat. Immunol. *23*, 177–185. https://doi.org/10.1038/s41590-021-01123-9.

Cohen, C.A., Li, A.P.Y., Hachim, A., Hui, D.S.C., Kwan, M.Y.W., Tsang, O.T.Y., Chiu, S.S., Chan, W.H., Yau, Y.S., Kavian, N., et al. (2021). SARS-CoV-2 specific T cell responses are lower in children and increase with age and time after infection. Nat. Commun. *12*, 4678. https://doi.org/10.1038/s41467-021-24938-4.

Collier, D.A., Ferreira, I.A.T.M., Kotagiri, P., Datir, R.P., Lim, E.Y., Touizer, E., Meng, B., Abdullahi, A., CITIID-NIHR BioResource COVID-19 Collaboration, Elmer, A., et al. (2021). Age-related immune response heterogeneity to SARS-CoV-2 vaccine BNT162b2. Nature *596*, 417–422. https://doi.org/10.1038/s41586-021-03739-1.

Cotugno, N., Ruggiero, A., Pascucci, G.R., Bonfante, F., Petrara, M.R., Pighi, C., Cifaldi, L., Zangari, P., Bernardi, S., Cursi, L., et al. (2021). Virological and immunological features of SARS-COV-2 infected children with distinct symptomatology. Pediatr. Allergy Immunol. *32*, 1833–1842. https://doi.org/10.1111/pai.13585.

Dash, P., Fiore-Gartland, A.J., Hertz, T., Wang, G.C., Sharma, S., Souquette, A., Crawford, J.C., Clemens, E.B., Nguyen, T.H.O., Kedzierska, K., et al. (2017). Quantifiable predictive features define epitope-specific T cell receptor repertoires. Nature *547*, 89–93. https://doi.org/10.1038/nature22383.

Delahoy, M.J., Ujamaa, D., Whitaker, M., O'Halloran, A., Anglin, O., Burns, E., Cummings, C., Holstein, R., Kambhampati, A.K., Milucky, J., et al. (2021). Hospitalizations associated with COVID-19 among children and adolescents - COVID-NET, 14 States, March 1, 2020–August 14, 2021. MMWR Morb. Mortal. Wkly. Rep. *70*, 1255–1260. https://doi.org/10.15585/mmwr.mm7036e2.

Dowell, A.C., Butler, M.S., Jinks, E., Tut, G., Lancaster, T., Sylla, P., Begum, J., Bruton, R., Pearce, H., Verma, K., et al. (2022). Children develop robust and sustained cross-reactive spike-specific immune responses to SARS-CoV-2 infection. Nat. Immunol. *23*, 40–49. https://doi.org/10.1038/s41590-021-01089-8.

Ferretti, A.P., Kula, T., Wang, Y., Nguyen, D.M.V., Weinheimer, A., Dunlap, G.S., Xu, Q., Nabilsi, N., Perullo, C.R., Cristofaro, A.W., et al. (2020). Unbiased screens show $CD8^+$ T cells of COVID-19 patients recognize shared epitopes in SARS-CoV-2 that largely reside outside the spike protein. Immunity *53*, 1095–1107.e3. https://doi.org/10.1016/j.immuni.2020.10.006.

Francis, J.M., Leistritz-Edwards, D., Dunn, A., Tarr, C., Lehman, J., Dempsey, C., Hamel, A., Rayon, V., Liu, G., Wang, Y., et al. (2022). Allelic variation in class I HLA determines CD8$^+$ T cell repertoire shape and cross-reactive memory responses to SARS-CoV-2. Sci. Immunol. *7*, eabk3070. https://doi.org/10.1126/sciimmunol.abk3070.

Gangaev, A., Ketelaars, S.L.C., Isaeva, O.I., Patiwael, S., Dopler, A., Hoefakker, K., De Biasi, S., Gibellini, L., Mussini, C., Guaraldi, G., et al. (2021). Identification and characterization of a SARS-CoV-2 specific CD8$^+$ T cell response with immunodominant features. Nat. Commun. *12*, 2593. https://doi.org/10.1038/s41467-021-22811-y.

Goenka, A., Halliday, A., Gregorova, M., Milodowski, E., Thomas, A., Williamson, M.K., Baum, H., Oliver, E., Long, A.E., Knezevic, L., et al. (2021). Young infants exhibit robust functional antibody responses and restrained IFN-γ production to SARS-CoV-2. Cell Rep. Med. *2*, 100327. https://doi.org/10.1016/j.xcrm.2021.100327.

Gu, Z., Gu, L., Eils, R., Schlesner, M., and Brors, B. (2014). Circlize implements and enhances circular visualization in R. Bioinformatics *30*, 2811–2812.

Habel, J.R., Nguyen, T.H.O., van de Sandt, C.E., Juno, J.A., Chaurasia, P., Wragg, K., Koutsakos, M., Hensen, L., Jia, X., Chua, B., et al. (2020). Suboptimal SARS-CoV-2-specific CD8$^+$ T cell response associated with the prominent HLA-A*02:01 phenotype. Proc. Natl. Acad. Sci. USA *117*, 24384–24391. https://doi.org/10.1073/pnas.2015486117.

Hsieh, L.E., Grifoni, A., Sidney, J., Shimizu, C., Shike, H., Ramchandar, N., Moreno, E., Tremoulet, A.H., Burns, J.C., and Franco, A. (2022). Characterization of SARS-CoV-2 and common cold coronavirus-specific T-cell responses in MIS-C and Kawasaki disease children. Eur. J. Immunol. *52*, 123–137. https://doi.org/10.1002/eji.202149556.

Jansen, A.G., Sanders, E.A., Hoes, A.W., van Loon, A.M., and Hak, E. (2007). Influenza- and respiratory syncytial virus-associated mortality and hospitalisations. Eur. Respir. J. *30*, 1158–1166. https://doi.org/10.1183/09031936.00034407.

Juno, J.A., Tan, H.X., Lee, W.S., Reynaldi, A., Kelly, H.G., Wragg, K., Esterbauer, R., Kent, H.E., Batten, C.J., Mordant, F.L., et al. (2020). Humoral and circulating follicular helper T cell responses in recovered patients with COVID-19. Nat. Med. *26*, 1428–1434. https://doi.org/10.1038/s41591-020-0995-0.

Koutsakos, M., Illing, P.T., Nguyen, T.H.O., Mifsud, N.A., Crawford, J.C., Rizzetto, S., Eltahla, A.A., Clemens, E.B., Sant, S., Chua, B.Y., et al. (2019). Human CD8$^+$ T cell cross-reactivity across influenza A, B and C viruses. Nat. Immunol. *20*, 613–625. https://doi.org/10.1038/s41590-019-0320-6.

Liao, B., Chen, Z., Zheng, P., Li, L., Zhuo, J., Li, F., Li, S., Chen, D., Wen, C., Cai, W., et al. (2021). Detection of anti-SARS-CoV-2-S2 IgG is more sensitive than anti-RBD IgG in identifying asymptomatic COVID-19 patients. Front. Immunol. *12*, 724763. https://doi.org/10.3389/fimmu.2021.724763.

Loske, J., Röhmel, J., Lukassen, S., Stricker, S., Magalhães, V.G., Liebig, J., Chua, R.L., Thürmann, L., Messingschlager, M., Seegebarth, A., et al. (2022). Pre-activated antiviral innate immunity in the upper airways controls early SARS-CoV-2 infection in children. Nat. Biotechnol. *40*, 319–324. https://doi.org/10.1038/s41587-021-01037-9.

Mallapaty, S. (2021). Kids and COVID: why young immune systems are still on top. Nature *597*, 166–168. https://doi.org/10.1038/d41586-021-02423-8.

Messaoudi, I., Guevara Patiño, J.A., Dyall, R., LeMaoult, J., and Nikolich-Zugich, J. (2002). Direct link between MHC polymorphism, T cell avidity, and diversity in immune defense. Science *298*, 1797–1800. https://doi.org/10.1126/science.1076064.

Minervina, A.A., Pogorelyy, M.V., Kirk, A.M., Crawford, J.C., Allen, E.K., Chou, C.H., Mettelman, R.C., Allison, K.J., Lin, C.Y., Brice, D.C., et al. (2022). SARS-CoV-2 antigen exposure history shapes phenotypes and specificity of memory CD8$^+$ T cells. Nat. Immunol. *23*, 781–790. https://doi.org/10.1038/s41590-022-01184-4.

Moratto, D., Giacomelli, M., Chiarini, M., Savarè, L., Saccani, B., Motta, M., Timpano, S., Poli, P., Paghera, S., Imberti, L., et al. (2020). Immune response in children with COVID-19 is characterized by lower levels of T-cell activation than infected adults. Eur. J. Immunol. *50*, 1412–1414. https://doi.org/10.1002/eji.202048724.

Moreews, M., Le Gouge, K., Khaldi-Plassart, S., Pescarmona, R., Mathieu, A.L., Malcus, C., Djebali, S., Bellomo, A., Dauwalder, O., Perret, M., et al. (2021). Polyclonal expansion of TCR Vβ 21.3$^+$ CD4$^+$ and CD8$^+$ T cells is a hallmark of multisystem inflammatory syndrome in children. Sci. Immunol. *6*, eabh1516. https://doi.org/10.1126/sciimmunol.abh1516.

Mudd, P.A., Minervina, A.A., Pogorelyy, M.V., Turner, J.S., Kim, W., Kalaidina, E., Petersen, J., Schmitz, A.J., Lei, T., Haile, A., et al. (2022). SARS-CoV-2 mRNA vaccination elicits a robust and persistent T follicular helper cell response in humans. Cell *185*, 603–613.e15. https://doi.org/10.1016/j.cell.2021.12.026.

Mullen, J.L., Tsueng, G., Latif, A.A., Alkuzweny, M., Cano, M., Haag, E., Zhou, J., Zeller, M., Hufbauer, E., Matteson, N., et al. (2020). outbreak.info. https://outbreak.info/.

Ndhlovu, Z.M., Kamya, P., Mewalal, N., Kløverpris, H.N., Nkosi, T., Pretorius, K., Laher, F., Ogunshola, F., Chopera, D., Shekhar, K., et al. (2015). Magnitude and kinetics of CD8$^+$ T cell activation during hyperacute HIV infection impact viral set point. Immunity *43*, 591–604. https://doi.org/10.1016/j.immuni.2015.08.012.

Neeland, M.R., Bannister, S., Clifford, V., Dohle, K., Mulholland, K., Sutton, P., Curtis, N., Steer, A.C., Burgner, D.P., Crawford, N.W., et al. (2021a). Innate cell profiles during the acute and convalescent phase of SARS-CoV-2 infection in children. Nat. Commun. *12*, 1084. https://doi.org/10.1038/s41467-021-21414-x.

Neeland, M.R., Bannister, S., Clifford, V., Nguyen, J., Dohle, K., Overmars, I., Toh, Z.Q., Anderson, J., Donato, C.M., Sarkar, S., et al. (2021b). Children and adults in a household cohort study have robust longitudinal immune responses following SARS-CoV-2 infection or exposure. Front. Immunol. *12*, 741639. https://doi.org/10.3389/fimmu.2021.741639.

Nguyen, T.H.O., Koutsakos, M., van de Sandt, C.E., Crawford, J.C., Loh, L., Sant, S., Grzelak, L., Allen, E.K., Brahm, T., Clemens, E.B., et al. (2021a). Immune cellular networks underlying recovery from influenza virus infection in acute hospitalized patients. Nat. Commun. *12*, 2691. https://doi.org/10.1038/s41467-021-23018-x.

Nguyen, T.H.O., Rowntree, L.C., Petersen, J., Chua, B.Y., Hensen, L., Kedzierski, L., van de Sandt, C.E., Chaurasia, P., Tan, H.-X., Habel, J.R., et al. (2021b). CD8$^+$ T cells specific for an immunodominant SARS-CoV-2 nucleocapsid epitope display high naive precursor frequency and TCR promiscuity. Immunity *54*, 1066–1082.e5. https://doi.org/10.1016/j.immuni.2021.04.009.

Nguyen, T.H.O., Sant, S., Bird, N.L., Grant, E.J., Clemens, E.B., Koutsakos, M., Valkenburg, S.A., Gras, S., Lappas, M., Jaworowski, A., et al. (2018). Perturbed CD8$^+$ T cell immunity across universal influenza epitopes in the elderly. J. Leukoc. Biol. *103*, 321–339. https://doi.org/10.1189/jlb.5MA0517-207R.

Niessl, J., Sekine, T., Lange, J., Konya, V., Forkel, M., Maric, J., Rao, A., Mazzurana, L., Kokkinou, E., Weigel, W., et al. (2021). Identification of resident memory CD8$^+$ T cells with functional specificity for SARS-CoV-2 in unexposed oropharyngeal lymphoid tissue. Sci. Immunol. *6*, eabk0894. https://doi.org/10.1126/sciimmunol.abk0894.

Oberhardt, V., Luxenburger, H., Kemming, J., Schulien, I., Ciminski, K., Giese, S., Csernalabics, B., Lang-Meli, J., Janowska, I., Staniek, J., et al. (2021). Rapid and stable mobilization of CD8$^+$ T cells by SARS-CoV-2 mRNA vaccine. Nature *597*, 268–273. https://doi.org/10.1038/s41586-021-03841-4.

O'Driscoll, M., Ribeiro dos Santos, G., Wang, L., Cummings, D.A.T., Azman, A.S., Paireau, J., Fontanet, A., Cauchemez, S., and Salje, H. (2021). Age-specific mortality and immunity patterns of SARS-CoV-2. Nature *590*, 140–145. https://doi.org/10.1038/s41586-020-2918-0.

Peng, Y., Mentzer, A.J., Liu, G., Yao, X., Yin, Z., Dong, D., Dejnirattisai, W., Rostron, T., Supasa, P., Liu, C., et al. (2020). Broad and strong memory CD4$^+$ and CD8$^+$ T cells induced by SARS-CoV-2 in UK convalescent individuals following COVID-19. Nat. Immunol. *21*, 1336–1345. https://doi.org/10.1038/s41590-020-0782-6.

Pierce, C.A., Preston-Hurlburt, P., Dai, Y., Aschner, C.B., Cheshenko, N., Galen, B., Garforth, S.J., Herrera, N.G., Jangra, R.K., Morano, N.C., et al. (2020). Immune responses to SARS-CoV-2 infection in hospitalized pediatric

and adult patients. Sci. Transl. Med. *12*, eabd5487. https://doi.org/10.1126/scitranslmed.abd5487.

Porritt, R.A., Paschold, L., Rivas, M.N., Cheng, M.H., Yonker, L.M., Chandnani, H., Lopez, M., Simnica, D., Schultheiß, C., Santiskulvong, C., et al. (2021). HLA class I-associated expansion of TRBV11-2 T cells in multisystem inflammatory syndrome in children. J. Clin. Invest. *131*, e146614. https://doi.org/10.1172/JCI146614.

Price, D.A., Asher, T.E., Wilson, N.A., Nason, M.C., Brenchley, J.M., Metzler, I.S., Venturi, V., Gostick, E., Chattopadhyay, P.K., Roederer, M., et al. (2009). Public clonotype usage identifies protective Gag-specific $CD8^+$ T cell responses in SIV infection. J. Exp. Med. *206*, 923–936. https://doi.org/10.1084/jem.20081127.

Procop, G.W., Brock, J.E., Reineks, E.Z., Shrestha, N.K., Demkowicz, R., Cook, E., Ababneh, E., and Harrington, S.M. (2021). A comparison of five SARS-CoV-2 molecular assays with clinical correlations. Am. J. Clin. Pathol. *155*, 69–78. https://doi.org/10.1093/ajcp/aqaa181.

Ramaswamy, A., Brodsky, N.N., Sumida, T.S., Comi, M., Asashima, H., Hoehn, K.B., Li, N., Liu, Y., Shah, A., Ravindra, N.G., et al. (2021). Immune dysregulation and autoreactivity correlate with disease severity in SARS-CoV-2-associated multisystem inflammatory syndrome in children. Immunity *54*, 1083–1095.e7. https://doi.org/10.1016/j.immuni.2021.04.003.

Rowntree, L.C., Chua, B.Y., Nicholson, S., Koutsakos, M., Hensen, L., Douros, C., Selva, K., Mordant, F.L., Wong, C.Y., Habel, J.R., et al. (2021a). Robust correlations across six SARS-CoV-2 serology assays detecting distinct antibody features. Clin. Transl. Immunology *10*, e1258. https://doi.org/10.1002/cti2.1258.

Rowntree, L.C., Petersen, J., Juno, J.A., Chaurasia, P., Wragg, K., Koutsakos, M., Hensen, L., Wheatley, A.K., Kent, S.J., Rossjohn, J., et al. (2021b). SARS-CoV-2-specific $CD8^+$ T-cell responses and TCR signatures in the context of a prominent HLA-A*24:02 allomorph. Immunol. Cell Biol. *99*, 990–1000. https://doi.org/10.1111/imcb.12482.

Sahin, U., Muik, A., Vogler, I., Derhovanessian, E., Kranz, L.M., Vormehr, M., Quandt, J., Bidmon, N., Ulges, A., Baum, A., et al. (2021). BNT162b2 vaccine induces neutralizing antibodies and poly-specific T cells in humans. Nature *595*, 572–577. https://doi.org/10.1038/s41586-021-03653-6.

Saini, S.K., Hersby, D.S., Tamhane, T., Povlsen, H.R., Amaya Hernandez, S.P.A., Nielsen, M., Gang, A.O., and Hadrup, S.R. (2021). SARS-CoV-2 genome-wide T cell epitope mapping reveals immunodominance and substantial $CD8^+$ T cell activation in COVID-19 patients. Sci. Immunol. *6*, eabf7550. https://doi.org/10.1126/sciimmunol.abf7550.

Schulien, I., Kemming, J., Oberhardt, V., Wild, K., Seidel, L.M., Killmer, S., Sagar, D., Daul, F., Salvat Lago, M., Decker, A., et al. (2021). Characterization of pre-existing and induced SARS-CoV-2-specific $CD8^+$ T cells. Nat. Med. *27*, 78–85. https://doi.org/10.1038/s41591-020-01143-2.

Selva, K.J., van de Sandt, C.E., Lemke, M.M., Lee, C.Y., Shoffner, S.K., Chua, B.Y., Davis, S.K., Nguyen, T.H.O., Rowntree, L.C., Hensen, L., et al. (2021). Systems serology detects functionally distinct coronavirus antibody features in children and elderly. Nat. Commun. *12*, 2037. https://doi.org/10.1038/s41467-021-22236-7.

Shomuradova, A.S., Vagida, M.S., Sheetikov, S.A., Zornikova, K.V., Kiryukhin, D., Titov, A., Peshkova, I.O., Khmelevskaya, A., Dianov, D.V., Malasheva, M., et al. (2020). SARS-CoV-2 epitopes are recognized by a public and diverse repertoire of human T cell receptors. Immunity *53*, 1245–1257.e5. https://doi.org/10.1016/j.immuni.2020.11.004.

Short, K.R., Kedzierska, K., and van de Sandt, C.E. (2018). Back to the Future: Lessons learned from the 1918 influenza pandemic. Back to the future. Front. Cell. Infect. Microbiol. *8*, 343. https://doi.org/10.3389/fcimb.2018.00343.

Toh, Z.Q., Anderson, J., Mazarakis, N., Neeland, M., Higgins, R.A., Rautenbacher, K., Dohle, K., Nguyen, J., Overmars, I., Donato, C., et al. (2022). Comparison of seroconversion in children and adults with mild COVID-19. JAMA Network Open *5*, e221313. https://doi.org/10.1001/jamanetworkopen.2022.1313.

Tosif, S., Neeland, M.R., Sutton, P., Licciardi, P.V., Sarkar, S., Selva, K.J., Do, L.A.H., Donato, C., Quan Toh, Z., Higgins, R., et al. (2020). Immune responses to SARS-CoV-2 in three children of parents with symptomatic COVID-19. Nat. Commun. *11*, 5703. https://doi.org/10.1038/s41467-020-19545-8.

Valkenburg, S.A., Josephs, T.M., Clemens, E.B., Grant, E.J., Nguyen, T.H.O., Wang, G.C., Price, D.A., Miller, A., Tong, S.Y.C., Thomas, P.G., et al. (2016). Molecular basis for universal HLA-A*0201-restricted $CD8^+$ T-cell immunity against influenza viruses. Proc. Natl. Acad. Sci. USA *113*, 4440–4445. https://doi.org/10.1073/pnas.1603106113.

van de Sandt, C.E., Clemens, E.B., Grant, E.J., Rowntree, L.C., Sant, S., Halim, H., Crowe, J., Cheng, A.C., Kotsimbos, T.C., Richards, M., et al. (2019). Challenging immunodominance of influenza-specific $CD8^+$ T cell responses restricted by the risk-associated HLA-A*68:01 allomorph. Nat. Commun. *10*, 5579. https://doi.org/10.1038/s41467-019-13346-4.

Wickham, H. (2016). ggplot2: Elegant Graphics for Data Analysis (Springer-Verlag).

Zhu, Y., Bloxham, C.J., Hulme, K.D., Sinclair, J.E., Tong, Z.W.M., Steele, L.E., Noye, E.C., Lu, J., Xia, Y., Chew, K.Y., et al. (2021). A meta-analysis on the role of children in severe acute respiratory syndrome coronavirus 2 in household transmission clusters. Clin. Infect. Dis. *72*, e1146–e1153. https://doi.org/10.1093/cid/ciaa1825.

STAR★METHODS

KEY RESOURCES TABLE

REAGENT or RESOURCE	SOURCE	IDENTIFIER
Antibodies		
CD71 M-A712 BV421	BD Biosciences	Cat#562995; RRID: AB_2737939
CD4 SK3 BV650	BD Biosciences	Cat#563875; RRID: AB_2744425
CD27 L128 BV711	BD Biosciences	Cat#563167; RRID: AB_2738042
CD38 HIT2 BV786	BD Biosciences	Cat#563964; RRID: AB_2738515
CCR7 150503 AF700	BD Biosciences	Cat#561143; RRID: AB_10562031
CD14 MΦP9 APC-H7	BD Biosciences	Cat#560180; RRID: AB_1645464
CD19 SJ25C1 APC-H7	BD Biosciences	Cat#560177; RRID: AB_1645470
CD45RA HI100 FITC	BD Biosciences	Cat#555488; RRID: AB_395879
CD8a SK1 PerCP-Cy5.5	BD Pharmingen	Cat#565310; RRID: AB_2687497
CD95 DX2 PE-CF594	BD Biosciences	Cat#562395; RRID: AB_11153666
PD-1 EH12.1 PE-Cy7	BD Biosciences	Cat#561272; RRID: AB_10611585
CD3 OKT3 BV510	BioLegend	Cat#317332; RRID: AB_2561943
HLA-DR L243 BV605	BioLegend	Cat#307640; RRID: AB_2561913
CD19 J4.119 ECD	Beckman Coulter	Cat#IM2708U; RRID:AB_130854
IgM G20-127 BUV395	BD Biosciences	Cat#563903; RRID:AB_2721269
CD21 B-ly4 BUV737	BD Biosciences	Cat#564437; RRID:AB_2738807
IgD IA6-2 PE-Cy7	BD Biosciences	Cat#561314; RRID:AB_10642457
IgG G18-145 BV786	BD Biosciences	Cat#564230; RRID:AB_2738684
CD27 O323 BV605	BioLegend	Cat#302829; RRID:AB_11204431
Streptavidin PE	BD Biosciences	Cat#349023, RRID:AB_2868860
Streptavidin APC	BD Biosciences	Cat#349024, RRID:AB_2868861
Streptavidin PE	Thermo Fisher Scientific	Cat#S866
Peroxidase AffiniPure goat anti-human IgG, Fcγ fragment specific	Jackson ImmunoResearch	Cat#109-035-098; RRID: AB_2337586
Rat anti-human IgA mAb MT20, alkaline phosphate-conjugated	MabTech	Cat#3860-9A; RRID: AB_10736550
anti-human IgM mAb MT22, biotinylated	MabTech	Cat#3880-6-250
Biological samples		
Blood samples (peripheral blood mononuclear cells (PBMCs) and plasma samples) from COVID-19 children and adults and healthy control individuals	Murdoch Children's Research Institute, Royal Children's Hospital, The University of Melbourne and Launceston General Hospital (Australia), Children's Hospital Los Angeles (USA)	N/A
Chemicals, peptides, and recombinant proteins		
3,3',5,5'-Tetramethylbenzidine (TMB) Liquid Substrate System for ELISA, peroxidase substrate	Sigma	Cat#T0440-1L
Alkaline phosphatase yellow (pNPP) liquid substrate for ELISA	Sigma	Cat#P7998-100ML
Pierce High Sensitivity Streptavidin-HRP	Thermo Fisher Scientific	Cat#21130
SARS-CoV-2 RBD, delta RBD and N proteins	Amanat et al., 2020	N/A
SARS-CoV-2 S2 protein	Sino Biologicals	Cat#40590-V08H1
SARS-CoV-2 Spike protein	Juno et al., 2020	N/A

(*Continued on next page*)

Continued

REAGENT or RESOURCE	SOURCE	IDENTIFIER
SARS-CoV-2 peptides – A1/ORF1a$_{1637}$ TTDPSFLGRY; A2/S269 YLQPRTFLL; A3/N$_{361}$ KTFPPTEPK; A24/S$_{1208}$ QYIKWPWYI; B7/N$_{105\text{-}113}$ SPRWYFYYL; B40/N$_{322}$ MEVTPSGTWL; and DPB4/S$_{167}$ TFEYVSQPFLMDLE	GenScript	N/A
HLA-A*01:01/ORF1a$_{1637}$ monomer (SARS-CoV-2, ORF1a$_{1637}$, TTDPSFLGRY)	Saini et al., 2021	N/A
HLA-A*03:01/N$_{361}$ monomer (SARS-CoV-2, N$_{361}$, KTFPPTEPK)	Peng et al., 2020	N/A
HLA-B*40:01/N$_{322}$ monomer (SARS-CoV-2, N$_{322}$, MEVTPSGTWL)	Peng et al., 2020	N/A
HLA-A*02:01/S$_{269}$ monomer (SARS-CoV-2, S$_{269}$, YLQPRTFLL)	Habel et al., 2020	N/A
HLA-B*07:02/N$_{105}$ monomer (SARS-CoV-2, N$_{105}$, SPRWYFYYL)	Nguyen et al., 2021b	N/A
HLA-A*24:02/S$_{1208}$ monomer (SARS-CoV-2, S$_{1208}$, QYIKWPWYI)	Nguyen et al., 2021b	N/A
HLA-DPA1*01:03/DPB1*04:01/S$_{167}$ monomer (SARS-CoV-2, S$_{167}$, TFEYVSQPFLMDLE)	Mudd et al., 2022	N/A
Software and algorithms		
R v3.6.2	The Comprehensive R Archive Network	https://cran.r-project.org
Circlize R package	Gu et al., 2014	https://cran.r-project.org/package=circlize
ggplot R package	Wickham, 2016	https://ggplot2.tidyverse.org
TCRdist pipeline	Dash et al., 2017	https://github.com/phbradley/tcr-dist
lme4 R package	Bates et al., 2014	https://www.jstatsoft.org/article/view/v067i01/
FlowJo v10.5.3	FlowJo	https://www.flowjo.com
Prism v8.3.1 or v9.1.0	GraphPad	https://www.graphpad.com
BD FACS Diva v8.0.1	BD Biosciences	https://www.bdbiosciences.com/en-us/instruments/research-instruments/research-software/flow-cytometry-acquisition/facsdiva-software
Other		
Anti-PE MicroBeads	Miltenyi Biotec	Cat# 130-048-801, RRID: AB_244373
Anti-APC MicroBeads	Miltenyi Biotec	Cat# 130-090-855, RRID: AB_244367

RESOURCE AVAILABILITY

Lead contact

Further information and requests for resources and reagents should be directed to and will be fulfilled by the lead contact, Katherine Kedzierska (kkedz@unimelb.edu.au).

Materials availability

This study did not generate new unique reagents.

Data and code availability

- TCR sequence data (Table S2) have been deposited into VDJdb [https://vdjdb.cdr3.net].
- The published article includes all datasets generated or analyzed during the study.
- This paper does not report original code.
- Any additional information required to reanalyze the data reported in this paper is available from the lead contact upon request.

EXPERIMENTAL MODEL AND SUBJECT DETAILS

Families experiencing COVID-19 symptoms and their household contacts were recruited at the Murdoch Children's Research Institute and Royal Children's Hospital (Victoria, Australia) from June 2020 to October 2021. The cohort consisted of 36 children (4 months-17 years) and 23 mothers (28-48 years). Due to HLA allele typing some families were excluded from the child-mother matched tetramer$^+$ T cell analysis (Figure 4). All but six children recruited into the household cohort were PCR$^+$ for SARS-CoV-2 as listed in Table S1. An additional cohort of SARS-CoV-2 PCR$^+$ children were recruited at the Children's Hospital Los Angeles (n=13, 1-14 years) between June 2020 and April 2021. SARS-CoV-2 PCR$^+$ adults were recruited from the community at convalescence (23-91 years). Individuals were determined to be symptomatic if they displayed 2 or more symptoms between days -2 to +14 of PCR testing. Pre-pandemic SARS-CoV-2-unexposed children and adults were recruited as healthy controls from Launceston General Hospital (Tasmania, Australia) and the University of Melbourne (Victoria, Australia). PBMCs were isolated from heparinized peripheral blood by Ficoll-Paque separation, plasma was collected for serology and DNA isolated from granulocytes was sent for HLA typing by VTIS (Victoria, Australia), essentially as described (Nguyen et al., 2021b). The demographics of all participants are listed in Table S1.

All human experimental work was conducted according to the Declaration of Helsinki principles and the Australian National Health and Medical Research Council Code of Practice. All blood donors or their legal guardians provided written informed consent. Ethics approval was granted from the Human Research Ethics Committee (HREC) of The Royal Children's Hospital (HREC/63666/RCHM-2019) for household families, the Children's Hospital Los Angeles (CHLA-20-00124) for the remaining COVID-19 exposed children, and the Tasmanian Health and Medical (H0017479) for healthy children donors. Human ethics was also granted from the Royal Melbourne Hospital HREC (HREC/66341/MH-2020) for COVID-19 exposed adults. Human ethics was also approved by the University of Melbourne (Ethics ID #1443389.4, #1955465, 2020-20782-12450-1, 2022-23719-25217-1).

METHOD DETAILS

SARS-CoV-2-specific antibodies and B cells

Assessment of IgM, IgG and IgA antibodies against SARS-CoV-2 (ancestral) RBD and N proteins were performed in-house by ELISA (Amanat et al., 2020; Nguyen et al., 2021b; Rowntree et al., 2021a). IgG antibodies were also assessed against S2 (Sino Biologicals) and delta RBD. Recombinant SARS-CoV-2 proteins (ancestral RBD, delta RBD and N) were produced using a mammalian cell protein expression system as described by Amanat et al. (2020). Absorbance for IgM and IgG titres were read at 450nm, while IgA was at 405nm. End-point titres were determined as essentially as described (Nguyen et al., 2021b; Rowntree et al., 2021a). Seroconversion of the children (0-17 years) and adults were defined when titres were above the mean plus 2 standard deviations of healthy non-COVID-19 children and adults, respectively.

Cells remaining from the TAME-flow through fractions (described below) were used to measure Spike-specific B cell responses, as described (Juno et al., 2020; Nguyen et al., 2021b), with Spike recombinant probes conjugated to PE fluorochromes. Stained cells were washed and fixed before acquisition on a BD LSRII Fortessa.

SARS-CoV-2 tetramer$^+$ T cell responses

HLA class I tetramers HLA-A*02:01/S_{269} (YLQPRTFLL), HLA-A*24:02/S_{1208} (QYIKWPWYI) and HLA-B*07:02/N_{105} (SPRWYFYYL) have previously been generated and validated as previously described (Habel et al., 2020; Nguyen et al., 2021b; Rowntree et al., 2021b). HLA-A*01:01/ORF1a$_{1637}$ (TTDPSFLGRY), HLA-A*03:01/N_{361} (KTFPPTEPK) and HLA-B*40:01/N_{322} (MEVTPSGTWL) class I tetramers were generated and validated using tetramer staining of T cell lines as described (Nguyen et al., 2021b). The HLA class II tetramer HLA-DPA1*01:03/DPB1*04:01/S_{167} (TFEYVSQPFLMDLE) was generated and validated essentially as described (Mudd et al., 2022).

One vial of cryopreserved PBMCs (5-10x10^6) were stained with a class I and/or class II SARS-CoV-2 tetramer on PE and/or another class I tetramer on APC. Cells underwent tetramer-associated magnetic enrichment (TAME) as described (Nguyen et al., 2021a, 2021b). Both class I and class II tetramers on PE were exclusively stained on CD8$^+$ or CD4$^+$ T cells, respectively, with minimal to zero non-specific binding. All flow-through fractions were negative for any remaining tetramer$^+$ cells and were cryopreserved for B cell analysis.

Following enrichment, tetramer$^+$ T cells were indexed single-cell sorted on a BD FACSAria III for TCR analysis essentially as described (Nguyen et al., 2021b). Multiplex-nested RT-PCR-amplified CDR3α and CDR3β regions from single cells (Nguyen et al., 2021b; Valkenburg et al., 2016) were analyzed by IMGT/V-QUEST.

QUANTIFICATION AND STATISTICAL ANALYSIS

TCR$\alpha\beta$ statistical analysis

Single-chain alpha and beta TCR sequences were paired through the TCRdist pipeline for modelling amino acid motifs, TCR landscapes, neighbour distance distribution and probabilities of generation (P_{gen}) (Dash et al., 2017). Previously published TCR datasets for B7/N_{105}, A2/S_{269}, and A24/S_{1208} were included in the analysis (Nguyen et al., 2021b; Rowntree et al., 2021b). Testing for variations in P_{gen} across epitope specificities was performed essentially as described (Nguyen et al., 2021b) using linear mixed

models (Bates, 2014). Data visualization for circos plots was performed in R using a package for circular layout (Gu et al., 2014)and graphics generation (Wickham, 2016). The subsampled and full repertoires are detailed in Table S2.

Amino acid sequence identity

Amino acid sequence identity of the viral peptides of the SARS-CoV-2 tetramers across the different VOC was determined using outbreak.info (Mullen et al., 2020). Mutations were reported in Figure S2B when the mutation was detected in $\geq$0.5% of the total sequences in the database for a single VOC (Bates et al., 2014; Dash et al., 2017; Valkenburg et al., 2016).

Statistical analysis

Statistical significance of nonparametric datasets (two-tailed) were determined using GraphPad Prism v9 software. Mann-Whitney U-test (unpaired) and Wilcoxon sign-rank test (paired) was used for comparisons between two groups. Kruskal-Wallis test (unmatched) with Dunn's multiple comparisons was used to compare more than two groups. Tukey's multiple comparison test compared row means between more than two groups, while Sidak's multiple comparison test compared column means between multiple groups.

Immunity, Volume *55*

Supplemental information

SARS-CoV-2-specific T cell memory with common TCR$\alpha\beta$ motifs is established in unvaccinated children who seroconvert after infection

Louise C. Rowntree, Thi H.O. Nguyen, Lukasz Kedzierski, Melanie R. Neeland, Jan Petersen, Jeremy Chase Crawford, Lilith F. Allen, E. Bridie Clemens, Brendon Chua, Hayley A. McQuilten, Anastasia A. Minervina, Mikhail V. Pogorelyy, Priyanka Chaurasia, Hyon-Xhi Tan, Adam K. Wheatley, Xiaoxiao Jia, Fatima Amanat, Florian Krammer, E. Kaitlynn Allen, Sabrina Sonda, Katie L. Flanagan, Jaycee Jumarang, Pia S. Pannaraj, Paul V. Licciardi, Stephen J. Kent, Katherine A. Bond, Deborah A. Williamson, Jamie Rossjohn, Paul G. Thomas, Shidan Tosif, Nigel W. Crawford, Carolien E. van de Sandt, and Katherine Kedzierska

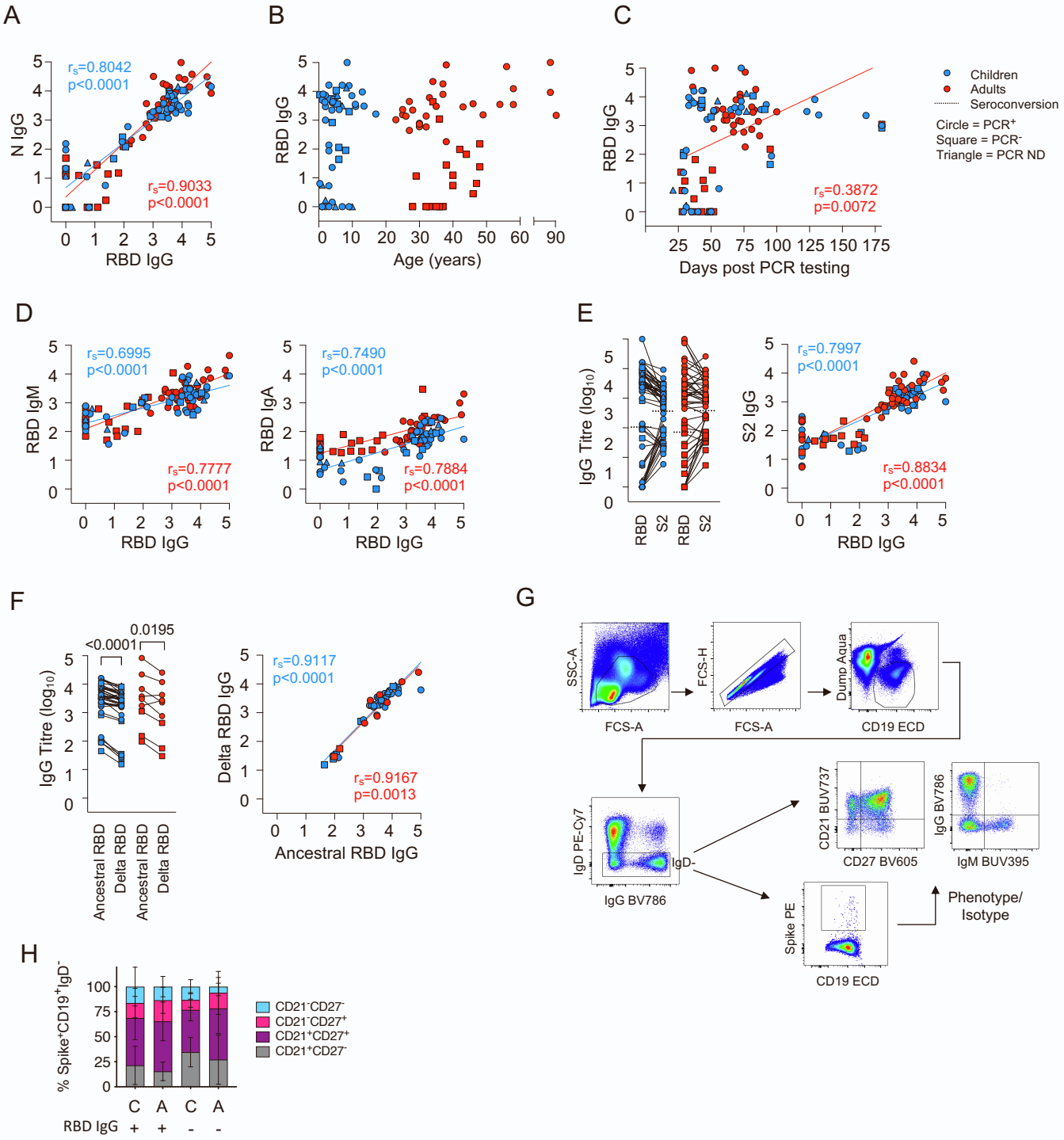

Figure S1. SARS-CoV-2-specific antibody and B cell response, refer to Figure 1. (A) Correlation between RBD IgG and N IgG titres for SARS-CoV-2 exposed children and adults. (B-C) Correlation between RBD IgG titres and (B) age or (C) days post PCR testing. (D) Correlation of RBD IgG titres against RBD IgM (left) and IgA (right). (E) Paired analysis (left) and correlation (right) of RBD- and S2-specific IgG antibody titres in SARS-CoV-2 exposed children and adults. Dashed lines indicate seroconversion cut-off based on healthy children and adult titres (mean plus two standard deviations). (F) Paired analysis (left) and correlation (right) of ancestral and delta RBD-specific IgG antibody titres. Statistical significance was determined using Wilcoxon matched-pairs signed rank test (E-F) and Spearman's rank correlation (A-F). (G) Gating strategy for Spike-specific B cells; gated on FSC/SSC, singlets, live cells excluding T cell/NK cell/monocyte lineage markers, expression of CD19, then gated as IgD^-, $IgM^{+/-}$, $IgG^{+/-}$ and binding to Spike probe, with expression of CD21/CD27. (H) Memory phenotypes of $Spike^+$ B cells from RBD IgG positive and negative individuals; data are shown as mean with SD. Statistical significance was determined with Sidak's multiple comparisons test.

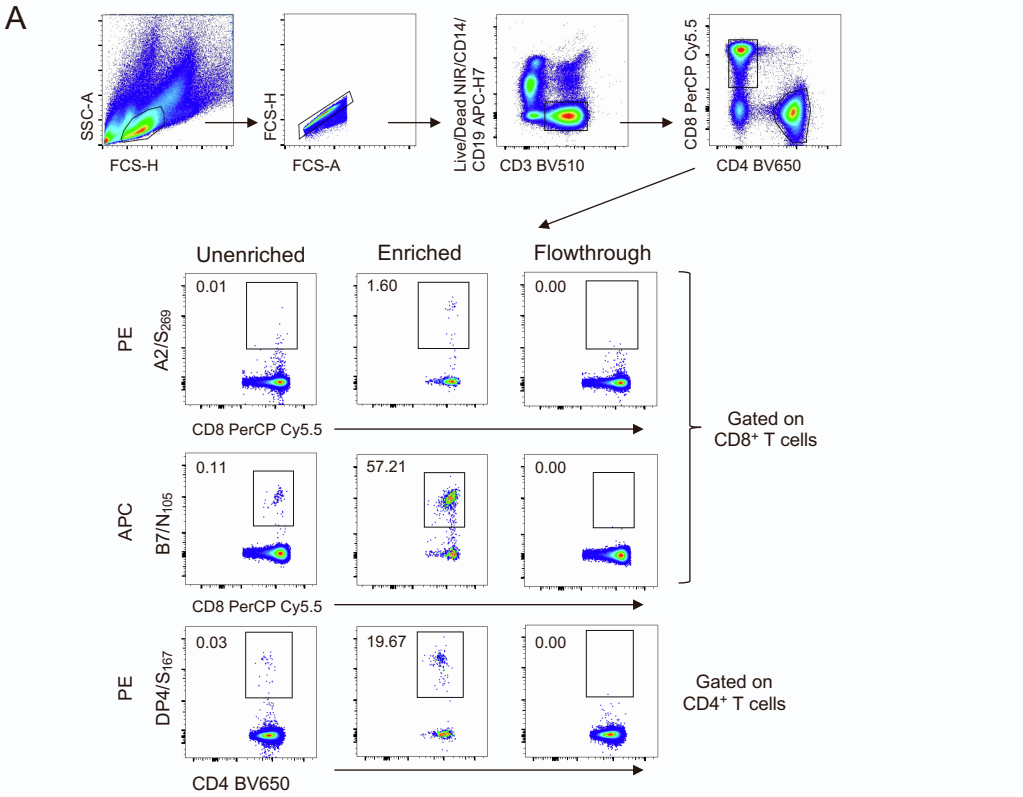

B

HLA	Region	Sequence tetramer	B.1.1.7 (Alpha)		B.1.351 (Beta)		P.1 (Gamma)		B.1.617.2 (Delta)		B.1.1.529 (Omicron)	
			Sequence	%	Sequence	%	Sequence	%	Sequence	%	Sequence	%
HLA-A*01:01	ORF1a$_{1637-1646}$	TTDPSFLGRY	----------	99.9	----------	99.9	----------	>99.9	----------	90.9	----------	>99.9
			---L------	0.1	---L------	0.1	---L------	<0.1	---L------	9.1	---L------	<0.1
HLA-A*02:01	S$_{269-277}$	YLQPRTFLL	---------	100	---------	100	---------	100	---------	100	---------	100
HLA-A*03:01	N$_{361-369}$	KTFPPTEPK	---------	99.9	---------	92	---------	99.9	---------	99.6	---------	99.9
			-I-------	0.1	-I-------	8	-I-------	0.1	-I-------	0.4	-I-------	0.1
HLA-A*24:02	S$_{1208-1216}$	QYIKWPWYI	---------	100	---------	100	---------	100	---------	100	---------	100
HLA-B*07:02	N$_{105-113}$	SPRWYFYYL	---------	100	---------	100	---------	100	---------	100	---------	100
HLA-B*40:01	N$_{322-331}$	MEVTPSGTWL	----------	99.9	----------	99.9	----------	99.8	----------	98.2	----------	100
			-----L----	0.1	-----L----	0.1	-----L----	0.2	-----L----	1.8	-----L----	0.1
HLA-DPB1*04:01	S$_{167-180}$	TFEYVSQPFLMDLE	----------	99.5	----------	>99.9	----------	>99.9	----------	>99.9	----------	100
			----------H--	0.5	----------H--	<0.1	----------H--	<0.1	----------H--	<0.1		

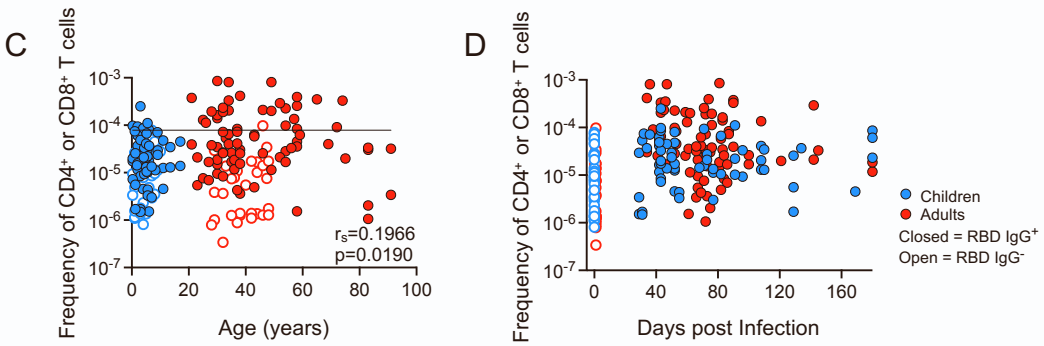

Figure S2. SARS-CoV-2-specific T cell frequencies and peptide conservation analysis, refer to Figure 2. (A) Gating strategy of enriched tetramer$^+$ CD4$^+$ and CD8$^+$ T cells and phenotype populations. (B) Amino acid sequence identity of the viral peptides of the SARS-CoV-2 tetramers across the different variants of concern (VOC). (C-D) Correlation of SARS-CoV-2 exposed individuals' frequency of tetramer$^+$ T cells against (C) age and (D) days post infection. Statistical significance was determined using Spearman's rank correlation.

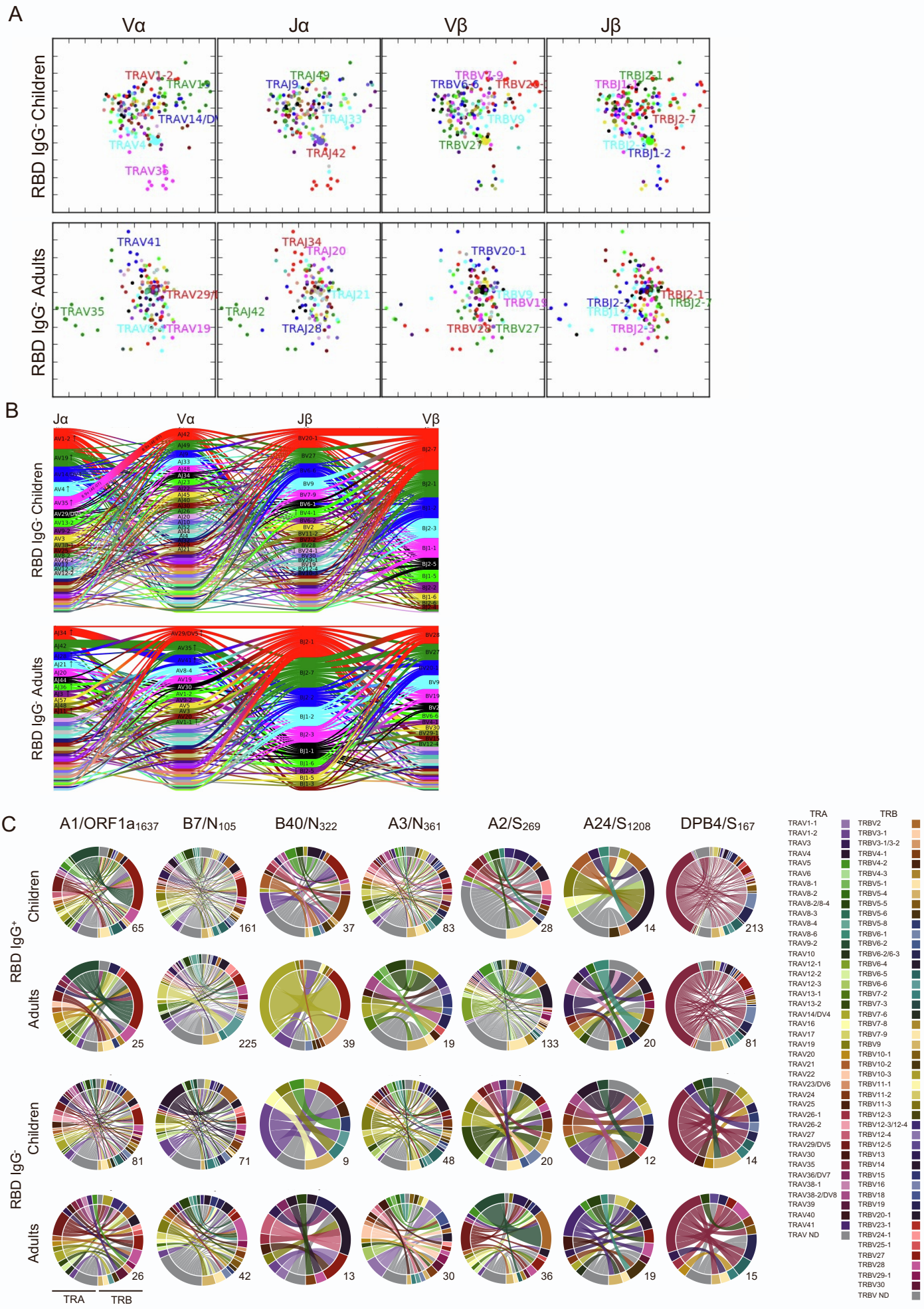

Figure S3 Rowntree*, Nguyen*, Kedzierski* et al

Figure S3. Diverse SARS-CoV-2-specific TCRab repertoires in RBD IgG$^-$ children and adults, refer to Figure 5. (A) Kernel PCA projections of pooled SARS-CoV-2-specific TCRs depicting Va, Ja, Vb, and Jb usage for RBD IgG$^-$ children and adults. Encoding clone size indicated by symbol size. (B) V and J gene segment usage and covariation in SARS-CoV-2-specific responses in RBD IgG$^-$ children and adults. (C) CIRCOS plots of TRAV and TRBV clonotype pairings in children and adults; left arch and segment color indicate TRAV usage, and right outer arch color depicts TRBV usage. Segments shown by the same color represent TCRab clonotypes with the same V segment usage but different CDR3 sequences. The number of sequences considered for each CIRCOS plot is shown at the bottom right.

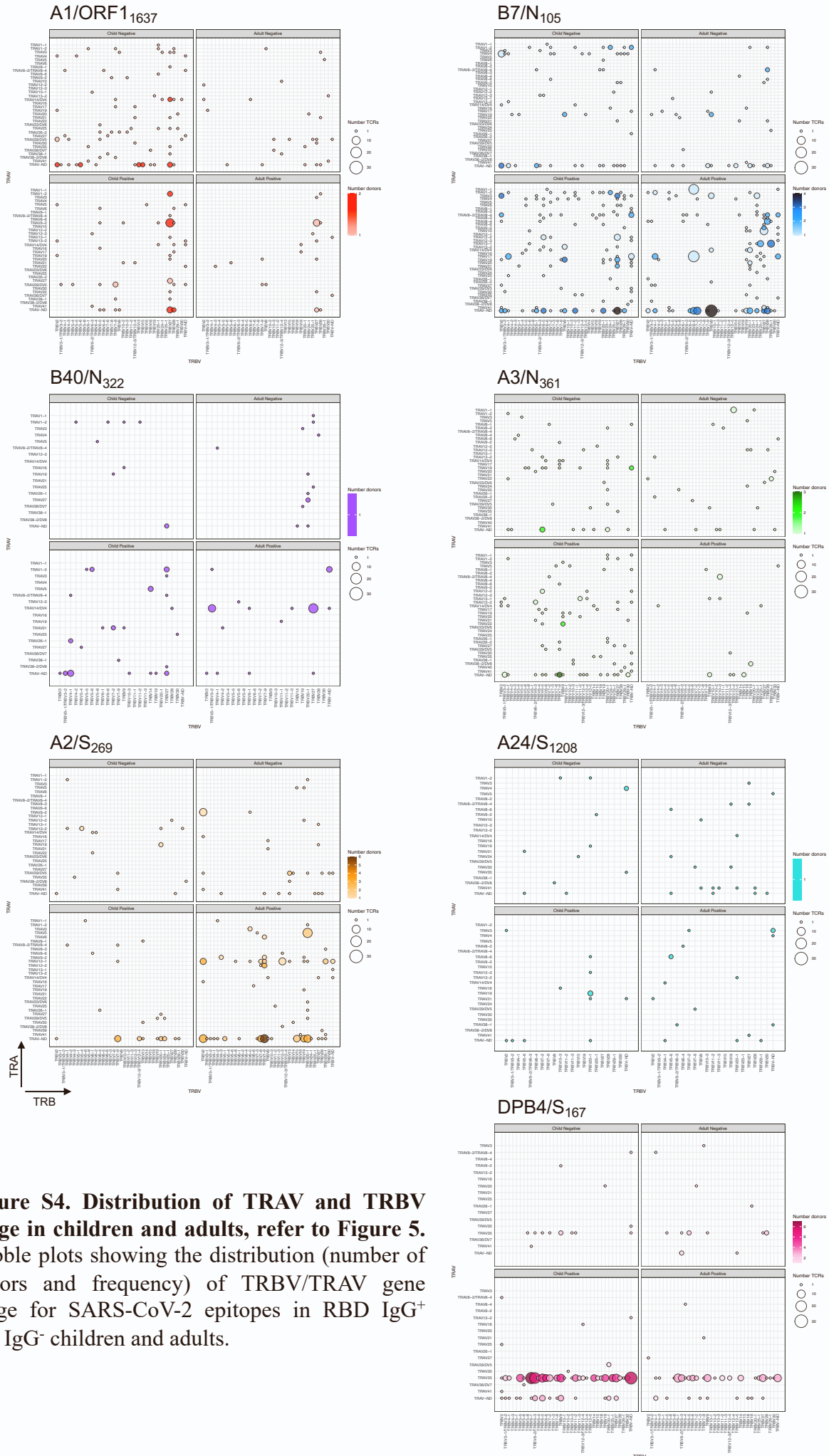

Figure S4. Distribution of TRAV and TRBV usage in children and adults, refer to Figure 5. Bubble plots showing the distribution (number of donors and frequency) of TRBV/TRAV gene usage for SARS-CoV-2 epitopes in RBD IgG^{+} and IgG^{-} children and adults.

A

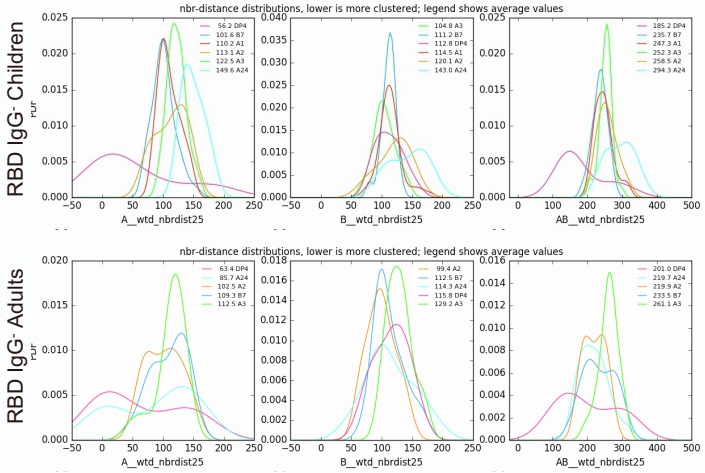

B

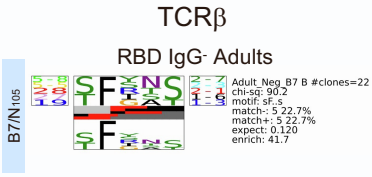

Figure S5. Similar distribution and probability of generation for SARS-CoV-2-specific TCRαβ repertories between RBD IgG$^-$ children and adults, refer to Figure 6. (A) Epitope-specific populations from RBD IgG$^-$ children and adults were quantified for defining features using a neighbour distance distribution. The lower distribution peak indicates a more clustered epitope-specific TCRab repertoire; average distance values for each epitope are depicted within the plot. Analyses for both single and paired chains are shown, as indicated in the plot labels. PFD, probability density function. (B) TCR logo representations of CDR3a and b sequence motif for RBD IgG$^-$ adults. The motif scores were determined by chi-squared, with values greater than 90 considered highly significant.

Supplementary Tables

Table S1. Cohort demographics, refer to Figure 1.

Cohort	Participant	Age (years)	Sex	RBD IgG ELISA	Symptomatic	Ct value*	Days post infection	HLA-A	HLA-A	HLA-B	HLA-B	HLA-DPB1	HLA-DPB1
MEL	9.2	40	F	-	-	-	28	02:01	11:02	07:02	27:04	03:01	05:01
MEL	9.3	3	M	-	+	e-Gene 32.44	30	02:05	11:02	27:04	58:01	05:01	104:01
MEL	18.2	44	F	-	-	-	38	02:01/614	68:01/164	40:01	49:01	04:01	104:01
MEL	18.3	7	M	-	+	e-Gene 40	40	01:01	02:01	49:01	50:01	04:01	104:01
MEL	21.2	29	F	-	+	-	30	02:01	25:01	07:02	18:01	04:01	
MEL	21.3	2	F	-	+	Inconclusive	31	03:01	25:01	18:01	50:01	04:01	04:02
MEL	25.2	47	F	-	-	-	45	02:01	11:01	07:02	44:02	01:01	15:01
MEL	25.4	10	F	-	+	Inconclusive	48	01:01	11:01	07:02	35:02	02:01	15:01
MEL	28.2	40	F	-	+	-	44	02:06	24:02	51:01	52NEW^	05:01	
MEL	28.3	5	M	-	+	Inconclusive	48	02:06	30:01	07:02	51:01	04:01	05:01
MEL	34.2	46	F	-	-	-	37	01:01	02:01	51:01	57:01	04:01	104:01
MEL	34.3	1	M	-	+	e-Gene 29.43	40	01:01	02:01	14:02	51:01	04:01	13:01
MEL	36.2	33	F	-	-	-	49	03:01	25:01	08:01	38:01	02:01	04:02
MEL	36.5	2	F	-	+	e-Gene 32.94	49	01:01	03:01	08:01	40:01	01:01	04:02
MEL	43.2	28	F	-	+	-	36	11:01	29:01	07:05	51:01	04:01	11:01
MEL	43.3	1	M	-	+	e-Gene 34.98	35	02:01	29:01	07:05	13:02	03:01	04:01
MEL	46.2	33	F	+	+	e-Gene 12.81	42	01:03	02:05	07:02	37:01	02:01	104:01
MEL	46.3	4	M	+	+	e-Gene 13.65	42	02:05	03:01	07:02	37:01	02:01	104:01
MEL	46.4	2	F	+	+	e-Gene 13.23	42	01:03	03:01	07:02		104:01	
MEL	52.1	38	F	-	+	-	51	02:01		44:02	51:01	04:01	
MEL	52.3	4	M	-	-	e-Gene 33.25	29	02:01	32:01	07:02	44:02	04:01	
MEL	52.4	1	F	-	+	Inconclusive	21	02:01	32:01	07:02	44:02	04:01	
MEL	53.1	37	F	-	-	-	43	02:01		15:01	39:01	03:01	04:01
MEL	53.4	0.33	M	-	+	e-Gene 36	56	01:01	02:01	15:01	51:01	03:01	
MEL	55.2	36	F	-	-	-	28	02:01	30:01	13:02	18:01	04:02	05:01
MEL	55.4	4	F	-	-	e-Gene 31.95	31	01:01	30:01	07:02	13:02	04:01	04:02
MEL	57.2	48	F	-	-	-	27	02:01	24:02	18:01	27:05	04:01	04:02
MEL	57.3	9	M	-	+	e-Gene 28.73	29	02:01		27:05	44:02	02:01	04:02
MEL	58.1	32	F	-	+	-	52	03:01	30:04	14:02		04:01	30:01
MEL	58.2	11	M	+	+	e-Gene 24.11	52	03:01	30:04	07:02	14:02	04:01	
MEL	58.3	6	M	+	-	e-Gene 24.25	52	03:01		07:02	14:02	04:01	30:01
MEL	61.3	46	F	+	+	-	59	24:02	24:10	35:30	40:01	01:01	13:01
MEL	61.5	17	M	+	-	e-Gene 25.45	47	24:02	24:33	40:01	51:06	01:01	
MEL	75.2	35	F	-	+	-	49	02:01	29:02	44:02	44:03	04:01	
MEL	75.3	3	F	-	+	e-Gene 27.37	50	01:01	29:02	37:01	44:03	04:01	
MEL	78.1	34	F	+	+	-	43	01:01	02:01	07:02	55:01	04:01	

MEL	78.3	3	M	+	+	-	43	01:01	02:01	07:02	08:01	04:01	
MEL	78.4	0.33	F	+	+	-	43	01:01	02:01	07:02	08:01	04:01	
MEL	80.1	42	F	-	-	-	29	02:01	24:02	07:02		04:01	06:01
MEL	80.3	6	F	+	-	-	29	24:02		07:02	27:04	04:01	06:01
MEL	80.4	8	F	-	-	-	29	24:02		07:02	27:04	04:01	06:01
MEL	80.5	3	M	+	+	e-Gene 33.77	31	02:01	30:02	07:02	18:01	02:02	04:01
MEL	84.1	48	F	+	-	-	95	02:03	11:01	38:02	39:05	02:02	296:01
MEL	84.3	3	M	-	-	e-Gene 31.22	96	11:01	32:01	28:02	44:02	04:01	296:01
MEL	84.4	6	M	-	-	-	95	02:03	24:02	07:02	39:05	02:01	02:02
MEL	88.1	35	F	+	+	-	100	02:01	26:01	35:08	38:01	04:01	
MEL	88.2	2	M	+	+	e-Gene 32.84	71	01:01	26:01	35:01	38:01	02:01	04:01
MEL	94.1	36	F	+	+	-	180	02:01	32:01	15:01	51:01	04:01	11:01
MEL	94.3	4	M	+	+	-	180	01:01	02:01	08:01	15:01	02:01	11:01
MEL	94.4	2	M	+	+	-	180	01:01	32:01	08:01	15:01	02:01	11:01
MEL	97.1	38	F	+	ND	-	35	02:01	03:01	07:02	57:01	02:01	26:01
MEL	97.3	2	F	+	+	-	35	03:01	11:01	52:01	57:01	02:01	
MEL	102.2	34	F	+	ND	-	36	01:01	26:01	08:01	38:01	02:01	09:01
MEL	102.3	13	M	+	+	E: 37.82, RDRP/S: N/A, N: 38.97	33	02:06	29:02	40:06	58:01	02:01	3:01
MEL	102.4	1	M	+	+	E: 14.36, RDRP/S: 15.67, N: 16.98	33	01:01		08:01	15:01	02:01	09:01
MEL	104.4	9	F	+	+	E: 20.08, RDRP/S: 21.50, N: 22.16	37	03:01	32:01	35:02	41:01	04:02	104:01:00
MEL	104.5	7	F	+	+	-	44	29:01		07:05		04:02	
MEL	104.6	5	M	+	+	E: 26.96, RDRP/S: 29.21, N: 29.85	37	29:01		07:05		04:02	
MEL	104.7	3	F	+	ND	-	43	03:01	29:01	07:05	35:02	04:02	
LA	HT1M6	4.36	F	+	+	N1 18.3, N2 20.8	92	02:01	11:01	35:01	38:01	04:01	
LA	HT34M5	3.93	M	+	-	N1 16.868, N217.882	168	30:01	32:01	15:01	52:01	04:01	04:02
LA	HT36M4	10.89	F	+	-	N1 32.8, N2 35.7	65	30:02	68:01	14:02	51:01	02:01	14:01
LA	HT47M1	5.02	M	+	+	N1 36, N2 36.4	88	02:01	03:01	07:02	18:01	04:01	105:01
LA	HT50M1	5.52	M	+	-	-	91	01:01	02:01	18:01	51:01	04:01	
LA	HT51M1	8.24	M	+	-	Inconclusive	77	24:02	68:01	35:12	39:11	04:02	14:01
LA	HT56M3	9.88	F	+	-	N1 31.3, N2 32.3	73						
LA	HT56M4	8.47	M	+	-	N1 31.7, N2 32.9	73	02:05	23:01	15:03	50:01	04:01	11:01
LA	HT59M1	1.27	F	+	+	N1 33.4, N2 35.4	129	02:01	68:03	07:02	39:05	04:01	04:02
LA	HT60M1	9.07	M	+	-	Undetected	50	01:01	02:06	07:02	15:30	02:01	04:02
LA	HT62M1	13.5	M	+	-	N1 34.1, N2 36.3	123	02:01	02:06	35:12	35:17	04:01	04:02
LA	HT64M1	5.59	F	+	+	Inconclusive	55	02:01	24:02	35:17	35:43	04:02	05:01
LA	HT66M5	4.21	M	+	-	N1 32.4, N2 35.9	73	03:01	11:01	39:01	44:02	03:01	04:02
LA	HT66M6	5.2	F	+	-	Undetected	82	02:01	68:03	35:01	39:01	04:01	04:02
LA	HT75M1	1.82	M	+	+	N1 24.6, N2 25	68	02:11	11:01	38:02	40:01	01:01	05:01
LA	HT83M1	6.98	F	+	-	Not tested	77	11:01	24:02	40:02	55:01	04:01	04:02

LA	HT93M1	6.09	F	+	+	N1 27.053, N2 28.464	132	29:02	32:01	18:01	44:03	04:01	131:01
MEL	CA01	25	M	+	+	NA	60	01:01	02:03	37:01	52:01	02:01	15:01
MEL	CA09	30	F	+	+	NA	67	02:01	23:01	49:01	49:01	702:01	14:01
MEL	CA12	23	M	+	+	NA	67	02:01	29:02	57:03	58:01	04:01	
MEL	CA16C1	30	F	+	+	NA	83	01:01	24:02	07:02	08:01	04:01	
MEL	CA17	49	F	+	+	NA	62	01:01	11:01	07:02	40:01	02:01	03:01
MEL	CA19	58	F	+	+	NA	53	02:01		07:02	15:01	04:02	04:02
MEL	CA21	32	F	+	+	NA	72	01:01	24:02	44:02	44:02	04:01	20:01
MEL	CA22	83	F	+	+	NA	75	24:02	33:01	14:02	55:01	04:01	05:01
MEL	CA23	83	F	+	+	NA	72	11:01	24:02	18:01	51:01	04:01	
MEL	CA27	58	F	+	+	NA	61	02:01	24:07	15:35	40:01	05:01	13:FNVU
MEL	CA29	25	F	+	+	NA	71	11:01	33:03	40:01	48:01	03:01	05:01
MEL	CA30	91	F	+	-	NA	66	24:02	26:01	15:01	38:01	02:01	04:01
MEL	CA33	28	F	+	+	NA	76	02:01		40:02	44:03	02:01	04:01
MEL	CA34C1	38	M	+	+	NA	73	03:01	24:02	07:02	52:01	03:01	04:01
MEL	CA35	26	F	+	+	NA	76	01:01	31:01	08:01	27:05	03:01	04:02
MEL	CA37C1	56	M	+	+	NA	54	02:01	26:01	44:02	47:01	02:01	05:01
MEL	CA38	54	F	+	+	NA	52	02:01	03:01	15:01	40:01	02:01	04:01
MEL	CA39	30	F	+	+	NA	81	01:01	02:01	08:01	27:05	04:01	04:02
MEL	CA46	27	M	+	+	NA	81	24:02		18:01	44:03	04:02	11:01
MEL	CA48	32	F	+	+	NA	84	02:01	29:02	14:01	37:01	04:01	11:01
MEL	CA52	27	F	+	-	NA	86	02:01	26:01	27:05	35:03	04:01	
MEL	CA52C1	37	M	+	+	NA	87	02:06	33:03	07:02	44:03	02:01	04:01
MEL	CA56	37	M	+	+	NA	69	01:01	02:01	35:03	40:01	02:01	04:02
MEL	CA61	43	F	+	+	NA	82	01:01	24:02	07:02	57:01	02:01	04:01

*Ct values were not available for some PCR-positive adults (NA) and were not obtained for PCR-negative adults or children (-).

^The new allele differs from 52:01:01:01 at codon 81 in exon 2 (GCG->GCT) resulting in no amino acid change.

ND, Not determined; NA, Not available.